The in-plane, elastic-plastic response of a filled hexagonal honeycomb at finite strain

J. Carlsson[a], K. Li[a,b], V. S. Deshpande[a] and N. A. Fleck[a*]

[a] Cambridge University Engineering Dept., Trumpington St., Cambridge, CB2 1PZ, UK

[b] Now at School of Mechanical Science and Engineering, Huazhong University of Science and Technology, Wuhan 430074, P. R. China

[*] Corresponding author. Email: naf1@eng.cam.ac.uk FAX: +44 12233 332662

1 August 2022

Abstract

Finite strain numerical solutions are derived for the in-plane, elastic-plastic response of a filled hexagonal honeycomb in uniaxial compression and in uniaxial tension. The cell walls and core are treated as elastic, ideally plastic von Mises solids, but the uniaxial strength of the core material is much less than that of the cell walls. The honeycomb has sides of equal length, and its inclined (but non-vertical) cell walls subtend an angle with respect to the transverse direction that can deviate from the usual value of +/-30° which is characteristic of a regular honeycomb. Two responses of the core are assumed: the fully bonded, 'non-cavitating core' (in the presence of a sufficiently high macroscopic pressure) and a 'cavitating core' that can cavitate or debond freely from the cell walls. When the honeycomb has cell walls that are inclined at 30° or less, the unit-cell response in uniaxial compression is stable and displays macroscopic hardening, regardless of whether the core can cavitate or not. In contrast, when the inclination of the cell walls exceeds 30°, the honeycomb with a cavitating core displays mild softening in uniaxial compression while the honeycomb with a non-cavitating core has a high initial yield strength, followed immediately by a strongly softening response. The strongly softening, isochoric mode occurs in an inclined shear band by the rotation of inextensional plastic hinges in the cell walls over a wavelength of two cells. A Maxwell construction is adequate for prediction of the propagation stress of the shear band in a finite specimen from a starter defect. Additional insight into the collapse mechanisms of the filled honeycomb (with a cavitating or non-cavitating core) is obtained via analytical solutions for a rigid, ideally plastic honeycomb, whereby the cell walls are treated as slender beams and the core has vanishing deviatoric strength. The full numerical solutions reveal that the filled honeycomb exhibits strong tension-compression asymmetry for both a cavitating core and a non-cavitating core.

Keywords: lattice materials, hexagonal honeycomb, plasticity, finite strain, shear band, collapse mechanisms

1. Introduction

A literature has emerged over the past 30 years on the mechanics of porous micro-architectured materials, also termed 'lattice materials' (Gibson and Ashby (1997); Ashby et al. (2000), Fleck et al. (2010)). Recently, the subject has had a major stimulus due to the emergence of nanoscale porous materials and of additive manufacture and rapid prototyping technologies, offering the possibility of 'material properties upon demand'. The voids within a lattice material are usually air-filled and, to first order, the mechanical properties of a lattice material depend upon its relative density. Additional opportunities exist for multi-phase lattices, such that the voids are filled with a solid or liquid to enhance macroscopic stiffness and strength, thermal or electrical conductivity, and so on. Only a very limited literature exists on lattices that have been filled with solids or fluids that are nearly incompressible yet possess a low deviatoric strength (see for example Tankasala et al. (2021), Shalchy et al. (2022) and Wang et al. (2020)), despite the fact that numerous biological examples exist of such filled lattices, e.g. adipose tissue (Comley and Fleck (2010); Comley and Fleck (2012)). An analysis of complex biological systems will require modifications to the approach adopted in the present basic study. For example, visco-elastic effects may be important and, at small scale, surface tension may also play a role.

A literature has been established on the in-plane compressive response of 2D and 3D lattice materials with a *compressible* foam core, see for example Cartie and Fleck (2003), Yan et al. (2013) and the recent review by Han et al. (2017). Synergistic strengthening can occur whereby the foam core stabilises the lattice against elastic or plastic buckling and changes the buckling mode. The structural benefit achieved by filling the air gaps of a lattice-cored sandwich panel with a ceramic or polymeric foam has also been explored, particularly for dynamic loading, see the recent review by Han et al. (2017). For the case of ballistic loading and shock loading, filling of the gaps between the struts of the lattice material adds mass to the sandwich structure and thereby reduces the kinetic energy of projectile and structure immediately following an inelastic impact event: this has been clearly demonstrated by the study of Wang et al. (2020) on the blast loading of a sandwich beam with a water-filled corrugated core. However, the water was contained in the corrugated core only by a weak sealing tape, and so the water was able to leak easily from the corrugated core and only provided minimal support of the lattice after initial impact. The existing literature does not address the collapse mechanisms of a 2D lattice under quasi-static in-plane loading by adding an incompressible fluid or solid of negligible deviatoric strength. This is a major objective of the present study.

A fundamental mechanics question is addressed in the present study: what is the effect upon the finite strain, in-plane response of a lattice material if its internal porosity is replaced by an incompressible solid of vanishing deviatoric strength, or equivalently by an incompressible, inviscid fluid? An initial attempt to address this question was made by Tankasala et al (2021). They analysed the small strain, elasto-plastic response of a fluid-filled hexagonal honeycomb and determined the sensitivity of shape of the yield surface to the inclination of the cell walls of the honeycomb. The macroscopic yield surface comprises several facets: some facets are associated with a weak, bending mode of collapse (macroscopic strength scaling quadratically with the relative density of the honeycomb) while other facets are dictated by a stronger, stretching mode (macroscopic strength scaling linearly with the relative density of the honeycomb). Tankasala et al (2021) also obtained closed form, analytical expressions for each facet of the in-plane yield-surface.

1.1 Scope of present study

The present study addresses the *finite strain*, elasto-plastic, uniaxial response of a filled hexagonal lattice. The sensitivity of macroscopic response to the presence/absence of core cavitation, cell wall inclination and relative density of the honeycomb is explored. An elastic, ideally plastic law is assumed for the hexagonal lattice, along with a much weaker elastic, ideally plastic response for the core. The significance of geometric hardening or softening is explored at finite strain, including the formation of crush bands and incompressible shear bands. The intent is to scope out the rich diversity of behaviour exhibited by the prototypical case of a 2D filled honeycomb.

It is fully anticipated that several of the above features will persist when the lattice and core strain harden, and for the 3D case of a *closed-cell* 3D lattice or foam. In a preliminary investigation (not reported here in any detail), the authors included the role of strain hardening in the core and cell walls of the honeycomb. It was found that the main features of macroscopic hardening and softening of the filled honeycomb were preserved when strain hardening was included. Thus, in order to highlight the major effects of geometric hardening and softening in dictating structural instabilities, and to make contact with analytical results such as those given by Tankasala et al. (2021), the authors chose to neglect the role of strain hardening in this initial study.

Now consider the relative behaviour of 2D and 3D lattices. The macroscopic response of a filled *open-cell* 3D lattice or foam is significantly different to that of the closed-cell 3D microarchitectured solid: in the 3D open-cell case, the solid or fluid that fills the porosity can migrate from cell to cell rather than remain contained within each representative cell. By way of example, consider the yield

response of an open-cell metallic foam, as characterised by the Deshpande and Fleck (2000) yield law. The empty foam strains macroscopically in a deviatoric manner, with no volume change, under macroscopic shear loading. Consequently, the addition of an inviscid, incompressible fluid to the foam has no effect upon its macroscopic response provided the fluid can migrate freely from one cell to the next through the random microstructure. Such inter-cell transport is prevented in a closed-cell 2D or 3D foam.

1.2 The filled hexagonal honeycomb: geometry and properties of constituents

The in-plane, elasto-plastic response of a filled hexagonal honeycomb, with cell walls of thickness t and length ℓ as shown in Fig. 1(a), is analysed by both finite element (FE) and upper bound analysis. The analytical model assumes rigid, ideally plastic beam theory for the cell walls, and an inviscid, incompressible core. In the finite element formulation, both the cell walls and the core comprise continuum elements made from elastic, ideally plastic von Mises solids. The cell walls possess a Young's modulus E_0 and yield strength σ_0, while the core has a Young's modulus E_C and yield strength σ_C. The yield strength and modulus of the core are taken to be less than those of the cell walls, such that $\sigma_C = 10^{-4}\sigma_0$ and $E_C = 10^{-4}E_0$. Consequently, the core has the same yield strain as that of the cell walls, $\varepsilon_0 = \sigma_0/E_0 = 0.001$. The Poisson's ratio of the cell walls and core equal 0.3 and 0.4999, respectively; thus, the core is almost incompressible, and the properties of the core can be taken to represent an incompressible, inviscid fluid. The cell walls have a density ρ_0, whereas the core has a density $\rho_C = 0.37\rho_0$ (to simulate a core of density comparable to that of water, gels or polymers, and cell walls made from an aluminium alloy, for example.) In general, the macroscopic loading rate is sufficiently slow for inertial effects to be negligible; however, when snap-back instabilities occur, material inertia plays a role in the transient dynamic response of the filled lattice, with wave reflections occurring throughout the structure. Attention is restricted to vanishing strain hardening in order to explore the significance of geometric hardening and softening as the filled honeycomb undergoes finite deformation under uniaxial tension or uniaxial compression.

The deformation of the honeycomb is determined in a Cartesian reference frame, with unit orthogonal base vectors $(\boldsymbol{e}_1, \boldsymbol{e}_2)$ as defined in Fig. 1(a). In the initial undeformed and stress-free configuration, the inclined cell walls of the hexagonal honeycomb subtend angles of ω_0 and $(\pi - \omega_0)$ with respect to the transverse direction; consequently, the elastic response of the honeycomb is transversely isotropic. We shall determine the uniaxial tensile and uniaxial compressive response of the filled honeycomb for 3 choices of cell wall inclination: ω_0= 20°, 30° and 40°. The choice ω_0= 30°

is isotropic in elastic response, and for the case of an empty honeycomb this choice of inclination defines an extremal hexagonal structure of lowest relative density for cell walls of fixed length ℓ. Honeycombs of inclination below the transition value of ω_0= 30°, such as choice ω_0= 20°, behave in one characteristic manner whereas honeycombs of inclination above the transition value, such as choice ω_0= 40°, behave in a different manner. It will also be shown that the qualitative collapse response in uniaxial tension and in uniaxial compression are sensitive to the inclination of cell walls, and to the possibility of core cavitation. Cavitation is due to either debonding of the core from the surrounding lattice of each unit cell, or to void nucleation and growth (Hill, 1950). Note that cavitation can be prevented by superposition of a sufficiently large macroscopic pressure. In the finite element simulations reported herein, the non-cavitating core is realised by ensuring that a void-free core remains fully bonded to the cell walls.

It is instructive to express the macroscopic, effective properties of the filled honeycomb in terms of the *relative density* $\bar{\rho}$ of the hexagonal lattice in the initial state, absent the contribution from the core; upon writing the volume of each hexagon in the undeformed state as $V_0 = 2\ell^2[(1 + \sin\omega_0)\cos\omega_0]$, the relative density is

$$\bar{\rho} = \frac{3t\ell}{V_0} = \frac{3t}{2\ell}[(1 + \sin\omega_0)\cos\omega_0]^{-1}, \qquad (1.1)$$

as detailed by Tankasala et al (2021), where ℓ is the side length of the side of the hexagon and t is the cell-wall thickness (Fig. 1a). The expression (1.1) for $\bar{\rho}$ achieves a minimum value at ω_0= 30°. In broad terms, it will be shown that the uniaxial tensile and compressive strength of the filled lattice scale as either $\bar{\rho}$ or $\bar{\rho}^2$, depending upon the activation of collapse modes of bar-stretching or bar-bending, respectively, following the notation of Deshpande et al. (2001).

2. Periodic unit cell response

Finite strain finite element (FE) simulations[1] of the collapse of filled and empty honeycombs were performed assuming plane strain deformation. Explicit calculations, with automatic time-stepping, were used to model the moving contact conditions of the cavitating core, to handle the large number of elements without excessive run times, to deal with snap-back instabilities in several cases, and to give accurate solutions when there is a large contrast between the strength of the core and that of the cell walls. Automatic mesh generation for both the cell walls and core employed a combination

[1] Abaqus/Explicit, version 6.14.1. Dassault Systèmes Simulia Corp., Providence, RI, USA.

of quadrilateral and triangular elements. Core cavitation was made possible by imposing frictionless contact between core and lattice. A non-cavitating response was achieved by imposing tie constraints on all core-lattice interfaces.

2.1 FE model and boundary conditions

First, the periodic unit cell response is reported for a representative volume element of width $W_C = 2\ell \cos\omega_0$ and height $H_C = 2\ell(1 + \sin\omega_0)$, as shown in Fig. 1(c). The unit cell contains two hexagons and can thereby capture the deformation of the infinite honeycomb over a wavelength of one or two hexagons: it will be confirmed in a subsequent section on the collapse of a large number of hexagons that the weakest collapse mode has a wavelength of one or two hexagons, depending upon the problem in hand.

Periodic boundary conditions were imposed on the boundaries of the unit cell as follows. Define two representative points A and B on opposing vertical sides of the unit cell and two representative points C and D on opposing horizontal sides of the unit cell (Fig. 1c). The macroscopic strain rate is specified via the following constraints,

$$\dot{u}_i^{\mathrm{B}} - \dot{u}_i^{A} = \dot{u}_{\mathrm{i},1}^{\infty} W_C, \quad \dot{u}_i^{\mathrm{D}} - \dot{u}_i^{\mathrm{C}} = \dot{u}_{\mathrm{i},2}^{\infty} H_C, \quad i = 1,2 \tag{2.1}$$

where the comma subscript 1 in $\dot{u}_{\mathrm{i},1}^{\infty}$ denotes differentiation with respect to X_1, and so on. Now impose a vanishing rotation rate to give

$$\dot{u}_1^{\mathrm{B}} - \dot{u}_1^{\mathrm{A}} = \dot{\varepsilon}_{11}^{\infty} W_C, \quad \dot{u}_2^{\mathrm{D}} - \dot{u}_2^{\mathrm{C}} = \dot{\varepsilon}_{22}^{\infty} H_B, \tag{2.2a}$$

and

$$(\dot{u}_2^{\mathrm{B}} - \dot{u}_2^{\mathrm{A}}) H_C = (\dot{u}_1^{\mathrm{C}} - \dot{u}_1^{\mathrm{D}}) W_C = \dot{\varepsilon}_{12}^{\infty} W_B H_B, \tag{2.2b}$$

where $\dot{\varepsilon}_{ij}^{\infty}$ is the nominal strain rate. The strain rate $\dot{\varepsilon}_{22}^{\infty} \equiv \dot{\varepsilon}^{\infty}$ is imposed while $\dot{\varepsilon}_{11}^{\infty}$ and $\dot{\varepsilon}_{12}^{\infty}$ serve as free, natural boundary conditions. Consequently, the periodic cell calculation delivers the macroscopic nominal stress component $\sigma_{22}^{\infty} \equiv \sigma^{\infty}$ which is work-conjugate to the nominal strain rate $\dot{\varepsilon}_{22}^{\infty} \equiv \dot{\varepsilon}^{\infty}$, and vanishing stress components σ_{11}^{∞} and σ_{12}^{∞} which are work-conjugate to $\dot{\varepsilon}_{11}^{\infty}$ and $2\dot{\varepsilon}_{12}^{\infty}$, respectively. In the simulations where a stable behaviour was observed, the macroscopic strain rate is sufficiently low that inertial effects play a negligible role. In other simulations, a snap-back instability was

observed and the response post peak-load involved transient wave effects. However, the peak load and the response subsequent to a few oscillations during the snap-back phase were unaffected by material inertia.

Both the cell walls and the core were meshed using first order reduced integration, 4-noded plane strain elements with hourglass control (CPE4R in ABAQUS notation), and supplemented by a small number of 3-noded plane strain elements (CPE3) to ensure that all space is filled. The lattice was discretised by a uniform mesh of element size equal to one fifth of the bar thickness t, which gave adequate accuracy according to a mesh convergence study (details not reported). The core was discretised into a non-uniform, graded mesh, of size on the order of $t/5$ near the cell walls and $\ell/10$ at the centre of each hexagon.

2.2 Reference cases: tensile and compressive responses of the empty honeycomb

First, consider the reference cases of the tensile and compressive responses of a periodic unit cell of empty honeycomb. The elasto-plastic deformation of the empty hexagonal honeycomb at both small and large strain is well-documented, see for example Papka and Kyriakides (1994), Gibson and Ashby (1997), and Tankasala et al. (2017). The collapse of empty honeycombs is by the formation of inextensional plastic hinges, see Fig. 2(b). Consequently, the macroscopic modulus and strength under uniaxial loading scale as $\bar{\rho}^3 E_0$ and $\bar{\rho}^2 \sigma_0$, respectively, with constants of proportionality that depend upon the cell wall inclination ω_0. At finite strain, a stable stiffening response is observed for uniaxial tension. In uniaxial compression, an unstable softening response occurs until opposing cell walls of the periodic unit cell make contact and volumetric lock-up ensues. These behaviours in tension and in compression are typified in Fig. 2 by plots of nominal stress σ^∞ versus nominal strain ε^∞ for the choice $t/\ell = 0.05$ and bar inclination ω_0 equal to 20°, 30° and 40°. The macroscopic yield strength of the empty honeycomb is almost identical in tension and in compression, consistent with the fact that the yield strain of the bars (and core) ε_0 is sufficiently small for finite strain effects (associated with cell wall rotation prior to yield) to be negligible and for elastic buckling not to intervene.

The macroscopic yield strength in tension and in compression increase by approximately 60% when ω_0 is increased from 20° to 40°. Post yield, the degree of geometric hardening in tension, and the degree of geometric softening in compression are greatest for $\omega_0 = 40°$. Mild softening persists for $-0.9 \leq \varepsilon^\infty \leq -0.6$, with volumetric lock-up absent, but this portion of the response has been omitted from the figure in order to highlight the initial behaviour. The simulations of compressive

response were continued until $\varepsilon^{\infty} \approx -0.9$ at which point the calculation gave excessive element distortion.

The mode of collapse for $\omega_0 = 40°$ is shown in Fig. 2(c) for uniaxial tension. Discrete hinges are evident, and their location is sketched in Fig. 2(b); this collapse mode occurs for all 3 values of ω_0 and for both tension and compression. It is clear from Fig. 2 that the softening behaviour in compression and stiffening in tension are associated with finite changes in geometry. The vertical bars remain vertical during tensile straining of the honeycomb, but undergo a symmetry-breaking mode of rotation during compressive straining, as first noted by Papka and Kyriakides (1994).

2.3 Tensile behaviour of filled honeycomb

The recent analysis by Tankasala et al. (2021) of a non-cavitating, filled honeycomb revealed that the small-strain tensile response is highly sensitive to the inclination angle ω_0. For the special case $\omega_0 = 30°$, initial yield is associated with the activation of inextensional plastic hinges and consequently σ_Y^{∞} scales as $\bar{\rho}^2\sigma_0$. For other choices of inclination angle ω_0, the macroscopic tensile yield strength σ_Y^{∞} additionally requires the plastic stretching of bars and consequently σ_Y^{∞} is proportional to $\bar{\rho}\sigma_0$, with the constant of proportionality depending upon the value of ω_0. With these features in mind, the finite tensile response is plotted in Fig. 3(a), using $\sigma^{\infty}/(\bar{\rho}\sigma_0)$ and ε^{∞} as axes. For the choice $t/\ell = 0.05$, the relative density $\bar{\rho}$ equals 0.0595, 0.0577 and 0.0596 for $\omega_0 = 20°, 30°$ and 40°, respectively. Predictions are shown both for a core that can cavitate and for a core that cannot cavitate.

The tensile response for $\omega_0 = 40°$ is insensitive to imposition of the constraint of no cavitation: as deformation proceeds, a positive (compressive) pressure develops within the core of the honeycomb. The yield strength σ_Y^{∞} is on the order of $0.3\ \bar{\rho}\sigma_0$, close to the value of $0.28\ \bar{\rho}\sigma_0$ for the collapse mode identified by Tankasala et al. (2021) using simple beam theory and discrete extensional plastic hinges in plane strain. Mild geometric hardening follows first yield, as shown in Fig. 3(a). An estimate of the pressure that is generated in the core is given by the small strain analysis of Tankasala et al. (2021). They considered the case of uniaxial tension and stated in their (7.7) that the pressure p is given by

$$\frac{p}{\sigma_0} = \frac{2}{3\sqrt{3}}\bar{\rho}\,\cos\omega_0 \cot\omega_0 \tag{2.3}$$

upon making suitable use of (1.1) and recognising that the macroscopic stress is elevated by the factor of $2/\sqrt{3}$ in plane strain. Recall that the present study is designed to determine the in-plane, plane strain

response a hexagonal lattice with cell walls in the form of plates that extend deep into the out-of-plane direction. This explains the need to elevate the strength of the cell walls from the simple beam solutions of Tankasala et al. (2021) by the factor of $2/\sqrt{3}$ to account for plane strain.

Likewise, for $\omega_0 = 30°$, the tensile response of the filled honeycomb with a core that can cavitate is identical to that of a non-cavitating core to within numerical accuracy. Initial yield occurs by the formation of inextensional plastic hinges in the bars as shown in Fig. 2(b), but subsequent deformation requires axial extension of the bars. Consequently, strong geometric hardening occurs as the honeycomb progressively aligns with the direction of tensile straining.

The case $\omega_0 = 20°$ is the most complex. The tensile response of the empty honeycomb is included in Fig. 3(a) and has the feature that tensile yield and subsequent plastic flow dilates the honeycomb. Consequently, the initial response of the filled honeycomb, but allowing for cavitation, is the same as that of the empty honeycomb. In contrast, imposition of the no-cavitation constraint on the core leads to a much higher yield strength σ_Y^{∞}, with plastic collapse requiring axial straining of bars in the plastic range; immediately following yield there is a switch in mechanism to a strongly softening mode that involves rotation of the vertical bars, as shown in Fig. 3(b). The arrangement of inextensional plastic hinges that give rise to this collapse mode is included in Fig. 3(b). The bars that were initially vertical first rotate in one direction and then reverse their direction of rotation until they become aligned again with the loading direction and strong hardening ensues.

Immediate insight into the tensile collapse mode of an empty honeycomb, or a filled honeycomb with a core that can cavitate for $\omega_0 < 30°$, is obtained by considering the volume V of each hexagon of the honeycomb as a function of current inclination angle ω. Assume that the honeycomb deforms by the rotation of inextensional plastic hinges such that ω increases under macroscopic tension and decreases under macroscopic compression. Then, at any stage of deformation, the volume V is given by

$$V/\ell^2 = \sin 2\,\omega + 2\cos\omega, \tag{2.4}$$

from (1.1); as already noted, V has a maximum at $\omega = 30°$. Consequently, an empty honeycomb of initial inclination $\omega_0 = 20°$ dilates under macroscopic tension until the bar inclination equals 30°. With continued tensile macroscopic straining, the bar inclination increases beyond 30° and shrinkage ensues. The lattice recovers its initial volume V_0 at a value ω_f that satisfies

$$\sin 2\omega_f + 2\cos\omega_f = \sin 2\omega_0 + 2\cos\omega_0\,, \qquad (2.5)$$

upon equating V in (2.4) to V_0 in (1.1). Thus, ω_f equals $39.68°$ for the choice $\omega_0 = 20°$. The above discussion has immediate implications for a honeycomb with a core of vanishing deviatoric strength that can cavitate: the filled honeycomb behaves in the same manner as an empty honeycomb until the point at which the volume of the hexagonal honeycomb recovers its initial value. At this instant volumetric lock-up occurs, and thereafter the filled honeycomb deforms in an incompressible manner.

2.4 Compressive behaviour of filled honeycomb

The compressive response of the periodic unit cell, for a cavitating and non-cavitating core, is shown in Fig. 4(a). Predictions are given for $t/\ell = 0.05$ and for the same values of $\omega_0 = 20°, 30°$ and $40°$ as for the tensile case. First, note that the compressive yield strength of the honeycomb with a non-cavitating core equals that of the tensile yield strength as the yield strain of the honeycomb lattice is sufficiently small for elastic buckling effects to be negligible.

The compressive responses of the honeycombs of inclination $\omega_0 = 20°$ and $30°$ are insensitive to imposition of the no-cavitation constraint: the compressive collapse mode of these filled honeycombs do not involve core cavitation. For the choice $\omega_0 = 20°$, initial yield occurs by stretching of the inclined bars. Mild geometric hardening follows this initial collapse, similar to that observed for the case of $\omega_0 = 40°$ in tension. Initial yield of the filled honeycomb of inclination $\omega_0 = 30°$ occurs by the formation of inextensional plastic hinges. Subsequent deformation involves axial stretching of bars and a strongly hardening response is observed post-yield.

The compressive response for $\omega_0 = 40°$ is sensitive to the imposition of the constraint of no cavitation in a similar manner to the tensile response of the honeycomb of $\omega_0 = 20°$, compare Figs. 4(a) and 3(a). Imposition of no cavitation endows the filled honeycomb with a high compressive yield strength of $0.28\bar{\rho}\sigma_0$ in plane strain, as predicted by Tankasala et al. (2021). A tensile hydrostatic stress is generated in the non-cavitating core of the honeycomb at the onset of yield; it is of equal magnitude to that given in (2.3) for tensile macroscopic loading but is opposite in sign. Thus, a macroscopic pressure that exceeds the value (2.3) is required to suppress cavitation in a $\omega_0 = 40°$ honeycomb under compressive loading.

Continue to consider the compressive response of a $\omega_0 = 40°$ non-cavitating filled honeycomb in the post-yield regime. A strongly softening response is exhibited, involving the symmetry-breaking

rotation of the vertical bars. Inextensional plastic hinges are formed, as sketched in Fig. 4(d). This response closely resembles that of the non-cavitating honeycomb of $\omega_0 = 20°$ tested in tension, compare Figs. 3(a) and 4(a), and compare Figs. 3(b) and 4(d). The compressive response of the empty honeycomb and of the filled honeycomb with a cavitating core are almost identical up to a compressive strain of about $\varepsilon^\infty = -0.15$: the filled honeycomb dilates and then shrinks until volumetric lock-up occurs at $\varepsilon^\infty = -0.15$. Lock-up of the empty honeycomb (by interference of cell-walls) occurs at a much larger value of macroscopic nominal strain between -0.9 and -1, beyond the regime of interest in Fig. 4(a). Note that the empty honeycomb and the honeycomb with a cavitating core both display mild geometric softening prior to lock-up.

2.5 Analytical model for compressive response of a honeycomb unit cell with a non-cavitating core

Tankasala et al (2021) have detailed the small-strain, in-plane collapse response of a honeycomb with a non-cavitating core; they used rigid, ideally plastic analysis and beam theory to obtain the exact solutions for the competing collapse modes that define the facets of the yield surface. Here, we extend their analysis into the finite strain regime for the uniaxial compression of a honeycomb of inclination ω_0 exceeding 30°, with a focus on the choice $\omega_0 = 40°$. The imposition of a non-cavitating core leads to an initial yield mode that involves axial stretch of both vertical bars and inclined bars, termed 'mode B' by Tankasala et al (2021), with macroscopic strength given by their (7.8) as

$$\frac{|\sigma^\infty|}{\bar{\rho}\sigma_0} \approx \frac{2(\sin\omega - \cos 2\omega)}{3\sqrt{3}\sin\omega}. \tag{2.6}$$

Note that a factor of $2/\sqrt{3}$ is included in (2.6) in order to give the plane strain solution, rather than the plane stress solution of Tankasala et al (2021). In this initial mode, the vertical bars do not rotate but are in a state of tensile yield. Tankasala et al (2021) explained in their section 7.2 that, in mode B, an extensional plastic hinge forms at each end of the vertical bars with a vanishing plastic moment due to the existence of a vertex in the moment-tension collapse locus for the hinge. Consequently, plastic bifurcation occurs immediately from mode B into a softening mode that involves rotation of the vertical bars. After a small rotation of the vertical bars (by less than 1 degree) this mode is replaced by a finite strain, incompressible version of the Gibson and Ashby (1997) shear mode of collapse.

The infinitesimal shear mode of Gibson and Ashby (1997) involves the rotation of the vertical cell walls from their initial inclination $\omega_3 = 90°$, and is an incompressible mode of deformation. However,

when this mode persists to finite strain, transverse and axial straining occurs at the macroscopic level. We emphasise that the correlation directions of this periodic mode of deformation are along the Cartesian base vectors $(\boldsymbol{e}_1, \boldsymbol{e}_2)$ as defined in Fig. 1. This finite strain response is summarised as follows.

Consider the plastic collapse of a hexagonal honeycomb of initial configuration $(\omega_1 = \omega_0, \omega_2 = \pi - \omega_0,\ \omega_3 = \pi/2)$, as shown in Fig. 1(a). (For analytical calculations, angles are specified in radians.) Inextensional plastic hinges develop in two of the three bars, with the inactive rigid bar changing as deformation proceeds, as explained below. The honeycomb deforms by the finite rotation of the three bars, while maintaining the symmetry of the two inclined bars $\omega_2 = \pi - \omega_1$, and constant volume $V = V_0$, where

$$V = 2\ell^2(\sin\omega_1 + \sin\omega_3)\cos\omega_1 = V_0. \tag{2.7}$$

Consequently, the bar inclination ω_3 can be expressed in terms of ω_1 as

$$\sin\omega_3 = \frac{\cos\omega_0 + \cos\omega_0 \sin\omega_0 - \cos\omega_1 \sin\omega_1}{\cos\omega_1}, \tag{2.8}$$

Also, the axial tensile component of macroscopic nominal strain ε^∞ is

$$\varepsilon^\infty = \frac{\sin\omega_1 + \sin\omega_3 - \sin\omega_0 - 1}{1 + \sin\omega_0}. \tag{2.9}$$

Insight into the collapse mode is obtained by considering (2.8) and (2.9). Take, as an example $\omega_0 = 40°$, and assume that collapse is by a monotonically decreasing value of ω_1. Then, ε^∞ becomes increasingly negative, while the transverse component of nominal strain ε_{11}^∞ increases in a positive manner by incompressibility. The dependence of ω_3 upon ω_1 is plotted in Fig. 5 for $\omega_0 = 40°$, upon making use of (2.8). The plot includes finite element predictions for the $\omega_0 = 40°$ honeycomb for the 3 types of core: non-cavitating, cavitating and empty. The finite element simulation for the non-cavitating core supports the mode (2.8). This collapse mode progresses as follows. As ω_1 decreases monotonically, (2.8) demands that ω_3 first decreases from 90°, and then attains a minimum value of ω_3=72.37° at ω_1=32.53°. Upon continued decrease of ω_1, the inclination ω_3 increases again until the collapse mechanism *locks-up* at the limiting value of $\omega_3 = 90°$; this occurs at $(1 + \sin\omega_1)\cos\omega_1 = (1 + \sin\omega_0)\cos\omega_0$ from (2.8), giving $\omega_1 = 19.64°$. We note in passing that this mechanism is reversible and also exists when the non-cavitating filled honeycomb is subjected to macroscopic tensile straining. For example, assume that the hexagonal honeycomb exists in an initial state such that

(ω_1=19.64°, $\omega_3 = 90°$); increase ω_1 in monotonic fashion and the trajectory of Fig. 5 is reversed. The honeycomb stretches in the axial x_2-direction until it locks up at (ω_1=40°, $\omega_3 = 90°$). The non-cavitating honeycomb of $\omega_0 = 20°$ deforms in tension by closely following this reverse path.

The collapse of a single horizontal row of hexagonal cells by this mode generates a non-monotonic finite macroscopic shear strain $\varepsilon_{12}^{\infty}$ within this band of cells; the shear strain attains a maximum value and then drops to zero at lock-up. If instead, the collapse mode involves a repeating stack of such rows of hexagons, with the collapse of each layer alternating in a *twinning* mode, then $\varepsilon_{12}^{\infty}$ vanishes at all stages of collapse of the overall stack. This alternating mode of collapse is observed in the FE simulations, see Fig. 4(d). However, the essential kinematics of (2.8) and (2.9) are preserved in the twinning mode.

Now equate the macroscopic work rate to the plastic dissipation associated with hinge rotation of the non-cavitating hexagonal lattice in the above shear mode. First, recall that the minimum plastic dissipation rate at any joint between 3 bars of rotation rate $(\dot{\omega}_1, \dot{\omega}_2, \dot{\omega}_3)$ is obtained when the rotation rate $\dot{\omega}_{\mathrm{J}}$ of the joint J equals that of the bar of intermediate rotation rate. We proceed by considering a representative joint of the hexagonal lattice of Fig. 1. Then, upon noting that the plastic moment M_P for a bar of thickness t is $M_P = \sigma_0 t^2/2\sqrt{3}$ in plane strain, the plastic dissipation rate at the representative joint is

$$\dot{W}^J = \frac{\sigma_0 t^2}{2\sqrt{3}} \left(\left|\dot{\omega}_1 - \dot{\omega}_{\mathrm{J}}\right| + \left|\dot{\omega}_2 - \dot{\omega}_{\mathrm{J}}\right| + \left|\dot{\omega}_3 - \dot{\omega}_{\mathrm{J}}\right| \right). \tag{2.10}$$

Each hexagon has 6 joints, and each joint is shared by 3 neighbouring hexagons. Consequently, the macroscopic plastic work rate $\dot{W}^P$ within 1 hexagonal cell equals $2\dot{W}^J$, and (2.10) gives

$$\dot{W}^P = \sigma^{\infty}\, \dot{\varepsilon}^{\infty}\, V_0 = \frac{\sigma_0 t^2}{\sqrt{3}} \left(\left|\dot{\omega}_1 - \dot{\omega}_{\mathrm{J}}\right| + \left|\dot{\omega}_2 - \dot{\omega}_{\mathrm{J}}\right| + \left|\dot{\omega}_3 - \dot{\omega}_{\mathrm{J}}\right| \right). \tag{2.11}$$

For the collapse mechanism under consideration, the bar of intermediate rotation rate (that dictates the joint rotation rate $\dot{\omega}_{\mathrm{J}}$) evolves with axial strain ε^{∞}, as follows. The ratio $\dot{\omega}_3/\dot{\omega}_1$ is given by the slope of the plot of ω_3 versus ω_1 in Fig. 5. Initially, when ω_1 is less than ω_0, we have $\dot{\omega}_3/\dot{\omega}_1$>1 and so $\dot{\omega}_{\mathrm{J}} = \dot{\omega}_1$. Upon substituting $\dot{\omega}_{\mathrm{J}} = \dot{\omega}_1$ into (2.11), and making use of $\dot{\omega}_2 = -\dot{\omega}_1$, along with the expression for $\dot{\omega}_3/\dot{\omega}_1$ as given by (2.8) in rate form, σ^{∞} is obtained from (2.11) as a function of the tracking parameter ω_1. Simultaneously, the nominal strain ε^{∞} is determined as a function of ω_1 from

(2.9), upon making use of (2.8). The initial segment of the σ^{∞} versus ε^{∞} curve is thereby obtained, with ω_1 serving as a tracking parameter.

It is useful to obtain an analytical asymptotic expression for the initial response of σ^{∞} versus ε^{∞} by expanding ω_3 about its initial value of $\pi/2$, such that $\omega_3 = (\pi/2)+\Delta\omega_3$, and likewise expanding ω_1 about its initial value of ω_0 such that $\omega_1 = \omega_0 + \Delta\omega_1$. Then, upon making suitable use of (2.8), (2.9) and (2.11) we obtain

$$\frac{-\sigma^{\infty}}{\bar{\rho}^2\sigma_0} = \frac{2}{9\sqrt{3}}(1+\sin\omega_0)\cos\omega_0\left(\frac{\sin\omega_0 - \cos 2\omega_0}{\sin\omega_0}\right)^{\frac{1}{2}}(-\varepsilon^{\infty})^{-\frac{1}{2}}, \qquad (2.12)$$

which is unbounded at $\varepsilon^{\infty} = 0$ and is strongly softening under increasing compressive strain. As mentioned above, Tankasala et al (2021) showed that initial plastic collapse by their 'mode B' involves axial yield of the vertical bars 3 and either inclined bars 1 or 2, with a collapse strength given by (2.6). Thus, we can use (2.6) as a cut-off for the collapse response (2.12) at a small value of compressive strain.

The relations (2.9) and (2.11) can also be used to obtain the dependence of σ^{∞} upon ε^{∞} at values of ε^{∞} for which $\dot{\omega}_3/\dot{\omega}_1$<1. Within the regime $-1 < \dot{\omega}_3/\dot{\omega}_1$<1, the minimum dissipation rate of the unit cell in (2.11) is attained by the choice $\dot{\omega}_J = \dot{\omega}_3$. The corresponding segment of the σ^{∞} versus ε^{∞} response is obtained by making use of (2.8), (2.9) and (2.11), and following the same procedure as that described above for the regime $\dot{\omega}_3/\dot{\omega}_1$>1. Likewise, consider the case $\dot{\omega}_3/\dot{\omega}_1 < -1$. Then, $\dot{\omega}_J = \dot{\omega}_2$ and (2.8), (2.9) and (2.11) give a third segment of the σ^{∞} versus ε^{∞} response up to the point of lock-up at (ω_1=19.64°, $\omega_3 = 90°$). The full σ^{∞} versus ε^{∞} response is included in Fig. 6 and agrees with the finite element predictions for a wide range of values of t/ℓ. We emphasise that this collapse mode requires the inextensional rotation of plastic hinges, and gives rise to a progressively increasing strain component $\varepsilon_{11}^{\infty}$ in the transverse direction and to shortening in the axial direction (negative value of ε^{∞}). Consequently, this mode cannot exist in the form of a localised shear band despite the fact that it gives rise to pronounced geometric softening.

2.6 Analytical model of compressive collapse of unit cell of honeycomb and a cavitating core

A relaxation of the non-cavitation constraint, such that collapse can be accompanied by dilatation of the honeycomb core, gives an additional degree of freedom for collapse of the unit cell. We continue to consider uniaxial compression of a honeycomb of inclination ω_0 exceeding 30°, with a focus on the

choice $\omega_0 = 40°$. Assume that plastic collapse occurs by the formation of plastic hinges associated with $\dot{\omega}_3 < 0$ and $-\dot{\omega}_2 = \dot{\omega}_1 < 0$. The σ^∞ versus ε^∞ response is again given by (2.9) and (2.11), but enforcement of $V = V_0$ is now relaxed by adopting the inequality $V \geq V_0$, to allow for cavitation of the core. The joint rotation rate $\dot{\omega}_J$ minimises σ^∞, and is obtained by considering all possibilities in turn: $\dot{\omega}_1 < \dot{\omega}_2 \leq \dot{\omega}_3$, $\dot{\omega}_1 < \dot{\omega}_3 < \dot{\omega}_2$ and $\dot{\omega}_3 \leq \dot{\omega}_1 < \dot{\omega}_2$. Upon making use of (2.11), we find that the choice $\dot{\omega}_3 = \dot{\omega}_1 = \dot{\omega}_J$ minimises σ^∞; the associated algebra is straightforward but tedious, and is omitted here for the sake of brevity. The honeycomb collapses with a single degree of freedom $\dot{\omega}_1$ when the core is allowed to cavitate, and (2.11) reduces to

$$-\sigma^\infty \dot{\varepsilon}^\infty V_0 = \left(2/\sqrt{3}\right)\dot{\omega}_1 \sigma_0 t^2 \,. \tag{2.13}$$

The dependence of σ^∞ upon ω_1 follows directly from (2.13) and (1.1) as

$$\frac{\sigma^\infty}{\bar{\rho}^2 \sigma_{YS}} = \frac{4}{9\sqrt{3}} \frac{(1+\sin\omega_0)^2 \cos\omega_0}{(\cos\omega_1 + \cos\omega_3)} \,, \tag{2.14}$$

along with

$$\omega_3 - \pi/2 = \omega_1 - \omega_0 \,, \tag{2.15}$$

from the identity $\dot{\omega}_3 = \dot{\omega}_1$; simultaneously, ε^∞ is prescribed as a function of ω_1 via (2.9). The initial yield strength follows directly from (2.14) as

$$\frac{\sigma^\infty}{\bar{\rho}^2 \sigma_{YS}} = \frac{4}{9\sqrt{3}} (1+\sin\omega_0)^2 \,, \tag{2.16}$$

This collapse mode has been identified previously by Papka and Kyriakides (1994) for an empty honeycomb. They performed a combined experimental and numerical study on an aluminium alloy honeycomb with vertical cell walls of double thickness, as a result of the manufacturing process. Papka and Kyriakides (1994) noted that the yield strength for this mode is identical to that of a symmetric mode of collapse ($\dot{\omega}_3 = 0, \dot{\omega}_2 = -\dot{\omega}_1$) of the empty honeycomb as given by Gibson and Ashby (1997), but the subsequent response has a steeper softening curve than that of the symmetric mode, and is consequently the dominant mode. Consistent with these findings, the yield strength stated in (2.16) is identical to that given by Gibson and Ashby (1997) for the symmetric mode of collapse.

The asymmetric collapse mode (2.11), as plotted in Fig. 5, involves an initial dilatation of the honeycomb before the volume decreases again to the initial value V_0. The value of ω_1 at which $V = V_0$ is determined from (2.7) and (2.15), giving $\omega_1 = 24.99°$ for $\omega_0 = 40°$. Subsequent deformation

occurs in an incompressible manner which is identical to that of the honeycomb that does not undergo cavitation.

The analytic model for the post-yield σ^{∞} versus ε^{∞} response of the cavitating $\omega_0 = 40°$ honeycomb agrees well with the stress versus strain curve obtained from unit cell finite element simulations, see Figs. 6(a) and (b). A comparison of the kinematics from the finite element simulations of the cavitating honeycomb and empty honeycomb is included in Fig 5; both the cavitating and empty honeycombs initially follow the prediction $\dot{\omega}_1 = \dot{\omega}_3$. At a strain of $\varepsilon^{\infty} \approx 0.15$, the volume of each hexagon has returned to its initial value and volumetric lock-up intervenes.

3. Finite specimen response

The periodic unit cell simulations of the $\omega_0 = 40°$ honeycomb with a non-cavitating core is strongly softening in uniaxial compression, recall Fig. 4(a). Despite this feature, the periodic unit cell mode of axial shortening and transverse stretching shown in Fig. 4(d) cannot give rise to a localisation band due to the finite straining parallel to the band. Inclined shear bands may exist provided they possess the property that extensional strain vanishes along the correlation direction of the band. The first step is to analyse the compressive response of a finite specimen of a $\omega_0 = 40°$ honeycomb to search for such modes.

3.1 Finite element simulations

Explicit finite element simulations were used to predict the compressive response of finite specimens made from 12 x 27 unit cells of hexagons of inclination $\omega_0 = 40°$; consequently, the rectangular specimen is of size 18ℓ x 89ℓ as shown in Fig. 7(a). The cells are empty or contain cores that are cavitating or non-cavitating; both the honeycomb and core are meshed using the same element types and sizes as detailed above for the periodic unit cell calculations. A single cell (edges and core) is removed at half-height on one side of the specimen in order to define an imperfection from which crush bands or shear bands can initiate, see Fig. 7(a). The sides of the specimen are traction-free, while the top and bottom faces are frictionless. The top face is subjected to a downward velocity $-\dot{u}^{\infty}/2$, while the bottom face is subjected to an upward velocity $\dot{u}^{\infty}/2$, where $\dot{u}^{\infty}$is sufficiently small for inertial effects to be negligible. Thus, the end shortening rate equals $\dot{u}^{\infty}$.

Representative solutions for the average compressive traction $-\langle\sigma^{\infty}\rangle$ versus non-dimensional end shortening u^{∞}/ℓ are given in suitably normalised form in Fig. 7(b) for the non-cavitating core, and in Fig. 7(c) for the cavitating core and empty core. A pronounced peak load exists for the honeycomb with non-cavitating core followed by a load plateau. In contrast, only mild softening follows the peak load for the honeycombs with a cavitating or empty core, Fig. 7(c). These contrasting collapse responses are indicative of very different collapse modes as follows.

The evolution of crush/shear bands in the finite specimen is shown in Fig. 8 for the three choices of core: (a) non-cavitating, (b) cavitating and (c) empty. The empty honeycomb both crushes and shears until it locks up when opposing cell walls interfere. However, the degree of axial shortening in Figs. 7(c) and 8(c) has not attained the required value for lock-up to occur and for the crush band to have fully formed; the structural collapse response of the finite specimen resembles that of the periodic unit cell, compare Figs. 2(a) and 7(c). This crush mode resembles that detailed previously by Papka and Kyriakides (1994), although its inclination of $\beta = 45°$ exceeds that observed by Papka and Kyriakides (1994); the inclination of the crush band in the empty honeycomb is sensitive to a number of factors including the width of the specimen, the relative density of the honeycomb and the yield strain of the cell walls. These details are beyond the scope of the present study.

The peak strength of the finite specimen made from a honeycomb with a cavitating core slightly exceeds that of the empty honeycomb due to the small contribution to macroscopic strength from the core, see Fig. 7(c). Volumetric lock-up of the cavitating core initiates in cells adjacent to the imperfection, at a load close to peak load of the filled, cavitating honeycomb. A shear band of inclination $\beta = 45°$ propagates across the net section of the specimen, and it contains cells which have locked-up to an incompressible state. After the shear band has propagated across the specimen, it spreads with continued end shortening of the specimen. However, the absence of a pronounced peak load at initiation of the shear band signifies that the collapse response resembles shear yielding with negligible strain hardening or softening, rather than a pronounced localisation event associated with a material instability.

The snap-back instability of the finite specimen containing a hexagonal lattice and a non-cavitating core is associated with the initiation of a shear band at an orientation of $\beta = 40°$. The shear band propagates across the width of the specimen, and then band-broadens at a constant macroscopic stress, as shown in Fig. 8(a). This behaviour is reminiscent of the behaviour of a microbuckle in a long fibre composite under axial compression, see for example Fleck (1997). The compressive strength of the finite specimen lies somewhat below that of the unit cell response, in part due to the presence of

the side-defect in the finite specimen, compare Figs. 6(b) and 7(b). However, the modes are very different: in the finite specimen a shear band develops, of inclination $\beta = 40°$ equal to that of the inclination ω_0 of the honeycomb.

3.2 Steady state propagation of a shear band

The nature of the shear band in the honeycomb with a non-cavitating core is now analysed. Recall from Fig. 8(a) that a shear band originates from the side-defect and propagates at almost constant net section stress which we shall denote by σ_P. The uniaxial compressive stress required to propagate an inclined shear band is estimated by a straightforward work calculation using the so-called Maxwell construction. The same approach has been used by Papka and Kyriakides (1994) to estimate the compressive stress to propagate a crush band in the transverse direction of an empty honeycomb. The classical Maxwell construction has also been used to calculate the steady state internal pressure required to inflate a cylindrical party balloon (Chater and Hutchinson, 1984), the external pressure on a cylindrical pipe to crush it along its axis (Kyriakides and Lee, 2021) and the propagation stress for a kink band in a long fibre composite (Fleck, 1997; Budiansky et al., 1998).

We emphasise that imposition of the constraint of no-cavitation of the core implies that the filled honeycomb behaves in an incompressible manner and localisation can only occur in the form of an inclined shear band, as sketched in Fig. 9(a). In steady state, the material upstream of the band is in a state A and possesses a shear strain γ_{A} while material within the shear band downstream from the tip is in a final, locked-up state B and possesses a shear strain γ_{B}. The steady state propagation stress τ_P is calculated by assuming that the work done in advancing the shear band, of width *w*, by a length δa is

$$\delta W = \tau_P(\gamma_{\mathrm{B}} - \gamma_{\mathrm{A}})w\delta a\,. \tag{3.1}$$

Equate this work to the plastic work done in shearing a volume $w\delta a$ of shear band material, in a shear band of width *w* and infinite length, from state A to state B, as sketched in Fig. 9(b):

$$\delta W = (\delta a)w\int_{\gamma_{\mathrm{A}}}^{\gamma_{\mathrm{B}}}\tau d\gamma\,. \tag{3.2}$$

A geometric construction for the propagation stress τ_P follows immediately: the area mapped out by $\tau_P(\gamma_{\mathrm{B}} - \gamma_{\mathrm{A}})$ equals the area mapped out by $\int_{\gamma_{\mathrm{A}}}^{\gamma_{\mathrm{B}}}\tau d\gamma$. Equivalently, the area *I* in Fig. 9(b) equals the area *II*. The axial propagation stress σ_P is directly related to the shear traction τ_P by $\tau_P =$

$0.5\sigma_P \sin 2\beta$ via rotation of axes by β. By simple kinematics, the propagation of the shear band across the width of the specimen gives rise to an axial shortening by $u^{\infty} = (\gamma_{\mathrm{B}} - \gamma_{\mathrm{A}}) w \sin\beta$.

3.3 Infinite band calculation

A periodic unit cell calculation is performed on the filled honeycomb with a non-cavitating core, as sketched in Fig. 10(a). Imagine that the shear band, of infinite length, contains many such unit cells across the width *w* of the shear band (as defined in Fig. 9(a)). The unit cell is subjected to a macroscopic simple shear strain on a plane inclined at $\beta = \omega_0$. Each unit cell contains two hexagons and is of height H_C and of width W_C, as shown in Fig 1(c). Corresponding locations on the left and right sides of the unit cell are denoted by points A and B, respectively, while corresponding locations on the bottom and top faces of the unit cell are again denoted by points C and D, respectively. The correlation direction of displacement is along the inclined direction of the shear band, and periodic displacement boundary conditions are applied whereby

$$\left(\dot{u}_i^{\mathrm{B}} - \dot{u}_i^{\mathrm{A}}\right) = \dot{\gamma} s_i W_C \sin\beta\,, \qquad \left(\dot{u}_i^{\mathrm{D}} - \dot{u}_i^{\mathrm{C}}\right) = \dot{\gamma} s_i H_C \cos\beta\,, \qquad i = 1,2. \tag{3.3}$$

Here, $\boldsymbol{s} = \boldsymbol{e}_1 \cos\beta - \boldsymbol{e}_2 \sin\beta$ is the unit vector parallel to the shear band, such that the direct component of macroscopic strain vanishes along the direction of $\boldsymbol{s}$.

The shear strain rate $\dot{\gamma}$ is imposed and the finite element solution delivers the work conjugate shear traction τ. Representative finite element results for $\tau(\gamma)$ are shown in Fig. 10(c) for the unit cell constrained to deform by simple shear along the direction of inclination $\beta = \omega_0 = 40^{\circ}$. Numerical experimentation reveals that the peak stress is $\tau_Y = 0.14\,\bar{\rho}\sigma_0$, and this is confirmed by an analytical beam analysis of the initial collapse response in Appendix A, with the main result presented in (A.17) for the small-strain collapse strength. For the sake of clarity, the analytical prediction (A.17) is compared with the early stages of finite element response in Fig. 10(d). Plastic bifurcation into a strongly softening bending mode occurs immediately at peak load, with inextensional plastic hinge formation as shown in Fig. 10(b). Finally, at a large value of shear strain $\gamma \approx 0.3$, the shear stress rises sharply again, see Fig 10(c). Collapse is bending-dominated as confirmed by the observation that the macroscopic shear stress $\tau(\gamma)$ scales with relative density squared in Fig. 10(c), upon assuming a range of values for the slenderness ratio of the bars. The propagation stress τ_P is obtained from $\tau(\gamma)$ for $\bar{\rho}$ in the range of 0.02 to 0.12, and an excellent fit gives $\tau_P = 0.44\bar{\rho}^{\,2}\sigma_0$; consequently, σ_P equals $0.9\bar{\rho}^{\,2}\sigma_0$ via traction equilibrium $\tau_P = 0.5\sigma_P \sin 2\beta$ where $\beta = \omega_0 = 40^{\circ}$. This estimate for σ_P is in

excellent agreement with the observed value of axial propagation stress in Fig. 7(b) for the finite specimen.

3.4 Finite specimen responses for tension and compression of filled honeycombs

For completeness, FE simulations were also performed on the compressive response of core-filled finite specimens of inclination $\omega_0 = 20^\circ$ and $\omega_0 = 30^\circ$, and on the tensile response of finite specimens of inclination $\omega_0 = 20^\circ, 30^\circ$ and 40°. The geometry and other details are the same as stated above in section 3.1. The results are consistent with the expectations from Figs. 2 and 3: a stable response with no localisation of deformation was observed except for (i) the case of section 3.1 that considered compressive loading of a finite specimen made from a honeycomb of inclination $\omega_0 = 40^\circ$ and a cavitating or non-cavitating core, and (ii) tensile loading of a finite specimen made from a honeycomb of inclination $\omega_0 = 20^\circ$ and a non-cavitating core. The results for the stable response of a finite specimen are not shown here, as they add little to the periodic unit cell responses already reported in Figs. 2 and 3. An initial study of the tensile response of the $\omega_0 = 20^\circ$ honeycomb with a non-cavitating core is given in Appendix B. It is again demonstrated that a Maxwell construction can again be used to estimate the propagation stress of the shear band.

4. Concluding remarks

The current study highlights the major effect of cavitation upon the tensile and compressive response of a filled hexagonal honeycomb. Cavitation results from either the spontaneous growth of voids in a weak core of the lattice when the hydrostatic stress in the core becomes positive, or by peeling of the core from the hexagonal lattice[2]. When cavitation can occur, the macroscopic tensile and compressive responses of the filled hexagonal honeycomb differ significantly. Consider, by way of example, the case where the inclination ω_0 equals 40°. If allowed to do so, the core will cavitate under uniaxial compression (recall Fig. 4(a)) but not under uniaxial tension (Fig. 3(a)): mild softening occurs in compression but geometric hardening occurs in tension. When the filled honeycomb is constrained against cavitation (for example by the superposition of a sufficiently large macroscopic pressure) a pronounced instability develops in a finite specimen under macroscopic compressive straining (recall Fig. 7(b)). Inclined shear bands initiate and propagate, first across the specimen and

[2] In the present study we assume that no resistance to cavitation exists in the form of a finite peel strength or a finite interfacial toughness.

then by band-broadening. The propagation stress is adequately predicted by analysing the simpler problem of an infinite shear band and by making use of the Maxwell construction. The mode of deformation within the shear band is bending-dominated and has a wavelength of two hexagons. In contrast, the non-cavitating honeycomb of inclination $\omega_0 = 40^\circ$ displays a stretching-dominated stable response under macroscopic tension, see Fig. 3(a). Geometric hardening precludes the possibility of a material instability.

The tension-compression asymmetry is reversed for the honeycomb whose inclined walls are initially at 20°. When this filled honeycomb is constrained against cavitation, it geometrically hardens in compression but undergoes severe softening in tension, associated with a switch in behaviour from stretching-governed deformation under macroscopic compression to bending-dominated shear band formation in macroscopic tension.

The above study has demonstrated that the filling of a cellular solid with a low-strength solid has a major effect upon its macroscopic response. Consequently, this opens up the possibility of a new class of multi-material micro-architectured solids that can be manufactured by additive or other methods. Additionally, the study raises important issues in the mechanics of biological tissues. For example, plant tissues are such cellular solids comprising stiff and strong cell walls made of cellulose that are filled with a fluid (the intracellular material). We have shown that cavitation is a distinct possibility when such materials are subjected to mechanical loads. The turgor pressure in plant cells will inhibit cavitation, although the analysis of the mechanical properties of plant tissues from such a perspective has received little attention.

Acknowledgements

The technical input of Dr. Harika Tankasala in the early stages of this project is appreciated. The authors are grateful for financial support from the European Research Council in the form of an Advanced Grant (MULTILAT, 669764).

References

Ashby, M.F., Evans, A.G., Fleck, N.A., Gibson, L.J., Hutchinson, J.W. and Wadley, H.N.G. (2000). Metal Foams: a Design Guide, Butterworth-Heinemann.

Budiansky, B., Fleck, N.A. and Amazigo, J.C. (1998). On Kink-Band Propagation in Fiber Composites, *J. Mech. Phys. Solids*, **46**(9), pp. 1637-1653.

Cartie D R and N A Fleck (2003). The effect of pin reinforcement upon the through-thickness compressive strength of foam-cored sandwich panels, *Composites Science and Technology*, **63**, 2401-2409.

Chater, E. and Hutchinson, J.W. (1944). On the propagation of bulges and buckles. *J. Appl. Mech*., **51**(2), pp. 269-277. https://doi.org/10.1115/1.3167611

Comley, K. and Fleck, N.A. (2010). A micromechanical model for the Young's modulus of adipose tissue. *Int. J. Solids Structs.* **47**, 2982-2990.

Comley, K. and Fleck, N.A. (2012). The compressive response of porcine adipose tissue from low to high strain rate. *Int. J. Impact Eng.* **46**, 1-10.

Deshpande, V.S. and Fleck, N.A. (2000). Isotropic constitutive models for metallic foams, *J. Mech. Phys. Solids*, **48** (6-7), pp 1253-1283.

Deshpande, V.S., Ashby, M.F. and Fleck, N.A. (2001). Foam topology: bending versus stretching dominated architectures. *Acta Materialia*, **49(6)**,1035-1040.

Fleck, N.A. (1997). Compressive failure of fibre composites, Advances in Applied Mechanics, **33**, Academic Press, eds. J.W. Hutchinson and T.Y. Wu, pp. 43-119.

Fleck, N.A., Deshpande, V.S. and Ashby, M.F. (2010). Micro-architectured materials: past, present and future. *Proc. Roy. Soc. A (London)*, **466**, 2495-2516.

Gibson, L. J. and Ashby, M. F. (1997). Cellular solids, structure and properties. 2nd. Edn. Cambridge University Press.

Guest, S. D. and Hutchinson, J.W. (2003). On the determinacy of repetitive structures. *J. Mech. and Phys. of Solids*, **51**, 383-391.

Han, B., Zhang, Z.J, Zhang, Q.C., Zhang Q. Lu, T.J. and Lu, B.H. (2017). Recent advances in hybrid lattice-cored sandwiches for enhanced multifunctional performance, *Extreme Mech. Lett*. **10**, 58-69.

Hill, R. (1950). Theory of plasticity, CUP.

Kyriakides, S. and Lee, L.H. (2021). On the propagation pressure of pipelines. Mechanics of Offshore Pipelines, Buckle Propagation and arrest, Vol. 2, Elsevier Inc. https://doi.org/10.1016/B978-0-12-817014-4.00002-1

Papka, S.D. and Kyriakides. S. (1994). In-plane compressive response and crushing of honeycomb. S. *J. Mech. Phys. Solids*, **42**(10), pp. 1499-1532.

Shalchy, F., Carlsson, J., Deshpande, V.S.D and Fleck, N.A. (2022). Pinching of gel-filled honeycomb, *Int. J. Solids Structs*., https://doi.org/10.1016/j.ijsolstr.2022.111728

Tankasala, H.C., Deshpande, V.S. and Fleck, N.A. (2017). Tensile response of elastoplastic lattices at finite strain. *J. Mech. Phys. Solids*, **109**, 307-330.

Tankasala, H.C., Deshpande, V.S. and Fleck, N.A. (2021). The in-plane elastic-plastic response of an incompressible, filled honeycomb. *J. Mech. Phys. Solids*, **155**, 104536. https://doi.org/10.1016/j.jmps.2021.104536.

Wang, X., Yu, R.P., Zhang, Q.C., Li, L., Li, X., Zhao, Z.Y., Han, B., He, S.Y. and Lu, T.J., (2020). Dynamic response of clamped sandwich beams with fluid-filled corrugated core, *Int. J. Impact Eng*. **139**, 103533.

Yan, L.L., Yu, B., Han, B., Chen, C.Q., Zhang Q.C. and Lu, T.J. (2013). Compressive strength and energy absorption of sandwich panels with aluminum foam-filled corrugated cores, *Comp. Sci. Tech*. **86**, 142-148.

Appendix A: Initial collapse mode of inclined shear band

Finite element simulations of the uniaxial compression of a finite specimen, with an imperfection in the form of a single broken and empty cell at the side face, reveal that the isochoric, non-cavitating honeycomb undergoes simple shear within a parallel-sided shear band. Deformation within the shear band is idealised by an infinite band finite element calculation, with the direction of shear parallel to one set of inclined bars of the honeycomb, see Fig. 10(a) for the initial, undeformed state and Fig. 10(b) for the deformed configuration. A finite shear strain develops within the band but with vanishing stretch along the band. The initial stage of this collapse mode entails the formation of an extensional plastic hinge in bar 3, and inextensional plastic hinges in bar 2, as sketched in Fig. A1. This is the same as 'mode B' in Tankasala et al (2021).

The initial, small strain, collapse mode of the shear band is now analysed using simple beam theory, along the same lines as that of Tankasala et al (2021), but now specialised to the case of simple shear along a band inclined at an angle $\beta = \omega_0$. First, the time rate of change of $(\omega_1, \omega_2, \omega_3)$ and of length ℓ_3 are determined as a function of the time rate of change of macroscopic shear strain γ in the band. The unit normal $\boldsymbol{n}$ to the band boundary and the unit vector along the band boundary $\boldsymbol{s}$, as defined in Fig. 10(a) and repeated in Fig. A1, are invariant with increasing deformation within the band, and are given by

$$\boldsymbol{n} = \boldsymbol{e}_1 \sin\omega_0 + \boldsymbol{e}_2 \cos\omega_0 \,, \quad \boldsymbol{s} = \boldsymbol{e}_1 \cos\omega_0 - \boldsymbol{e}_2 \sin\omega_0. \tag{A.1}$$

Four representative joints A-D are defined in Fig. A1. Note that the joints A and C are similarly situated within the hexagonal lattice, as are joints B and D. Joints A and C, with position vectors x_i^{A} and x_i^{C}, respectively, move to locations A' and C' in the deformed configuration with position vectors $x_i^{\mathrm{A}'}$ and $x_i^{\mathrm{C}'}$, respectively. The displacement of joints A and C are $u_i^{\mathrm{A}} = x_i^{\mathrm{A}'} - x_i^{\mathrm{A}}$ and $u_i^{\mathrm{C}} = x_i^{\mathrm{C}'} - x_i^{\mathrm{C}}$, respectively. The kinematics of the infinite band demand that $\left(x_i^{\mathrm{C}'} - x_i^{\mathrm{A}'}\right)$ is related to $\left(x_i^{\mathrm{C}} - x_i^{\mathrm{A}}\right)$ by the macroscopic shear strain γ parallel to the band according to

$$\left(x_i^{\mathrm{C}'} - x_i^{\mathrm{A}'}\right)n_i = \left(x_i^{\mathrm{C}} - x_i^{\mathrm{A}}\right)n_i \,, \tag{A.2}$$

and

$$\left(u_i^{\mathrm{C}'} - u_i^{\mathrm{A}'}\right)s_i = \gamma\left(x_i^{\mathrm{C}} - x_i^{\mathrm{A}}\right)n_i \,, \tag{A.3}$$

where

$$\boldsymbol{x}^{\mathrm{C}'} - \boldsymbol{x}^{\mathrm{A}'} = \ell_1(\boldsymbol{e}_1 \cos\omega_1 + \boldsymbol{e}_2 \sin\omega_1) + \ell_3(\boldsymbol{e}_1 \cos\omega_3 + \boldsymbol{e}_2 \sin\omega_3)\,, \tag{A.4}$$

and

$$\boldsymbol{x}^{\mathrm{C}} - \boldsymbol{x}^{\mathrm{A}} = \ell(\boldsymbol{e}_1 \cos\omega_0 + \boldsymbol{e}_2 \sin\omega_0) + \ell\boldsymbol{e}_2\,. \tag{A.5}$$

In similar fashion, the relative position of joints B′ and D′ in the deformed configuration is related to the initial relative position of B and D according to

$$\left(x_i^{\mathrm{D}'} - x_i^{\mathrm{B}'}\right)n_i = (x_i^{\mathrm{D}} - x_i^{\mathrm{B}})n_i\,, \tag{A.6}$$

and

$$\left(u_i^{\mathrm{D}'} - u_i^{\mathrm{B}'}\right)s_i = \gamma(x_i^{\mathrm{D}} - x_i^{\mathrm{B}})n_i\,, \tag{A.7}$$

where

$$\boldsymbol{x}^{\mathrm{D}'} - \boldsymbol{x}^{\mathrm{B}'} = \ell_1(\boldsymbol{e}_1 \cos\omega_1 + \boldsymbol{e}_2 \sin\omega_1) - \ell_2(\boldsymbol{e}_1 \cos\omega_2 + \boldsymbol{e}_2 \sin\omega_2)\,, \tag{A.8}$$

and

$$\boldsymbol{x}^{\mathrm{D}} - \boldsymbol{x}^{\mathrm{B}} = 2\boldsymbol{e}_1\ell\cos\omega_0. \tag{A.9}$$

The 4 relations (A.2), (A.3), (A.6) and (A.7) are used to solve for $(\omega_1, \omega_2, \omega_3)$ and the length ℓ_3 as a function of the macroscopic shear strain γ, upon assuming that bars 1 and 2 do not stretch, $\ell_1 = \ell_2 = \ell$. Substitution of (A.1), (A.4) and (A.5) into (A.2) gives

$$\ell\sin(\omega_0 + \omega_1) + \ell_3\sin(\omega_0 + \omega_3) = \ell\cos\omega_0\,(1 + 2\sin\omega_0)\,, \tag{A.10}$$

while insertion of (A.1), (A.4) and (A.5) into (A.3) gives

$$\begin{aligned}\ell\cos(\omega_0 + \omega_1) + \ell_3\cos(\omega_0 + \omega_3)\\ = \gamma\ell\cos\omega_0\,(1 + 2\sin\omega_0) + \ell\cos 2\omega_0 - \ell\sin\omega_0\,.\end{aligned} \tag{A.11}$$

In similar fashion, insertion of (A.1), (A.8) and (A.9) into (A.6) and (A.7), respectively, gives

$$\sin(\omega_0+\omega_1)-\sin(\omega_0+\omega_2)=\sin 2\omega_0\,, \tag{A.12}$$

and

$$\cos(\omega_0+\omega_1)-\cos(\omega_0+\omega_2)=\gamma\sin 2\omega_0+2\cos^2\omega_0. \tag{A.13}$$

Equations (A.10) – (A.13) are used to determine $(\omega_1,\omega_2,\omega_3,\ell_3)$ as a function of γ. We seek a small strain solution for the rigid, ideally plastic collapse state, and so (A.10) – (A.13) are linearised by writing them in rate form. Routine algebraic manipulation gives

$$\dot\omega_1=-\dot\gamma,\;\; \dot\omega_2=\dot\gamma\cos 2\omega_0,\;\; \dot\omega_3=-\dot\gamma(\cos^2\omega_0+\sin\omega_0\cos 2\omega_0), \tag{A.14}$$

and

$$\dot\ell_3=\dot\gamma\ell\cos\omega_0\,(\cos 2\omega_0-\sin\omega_0). \tag{A.15}$$

The shear traction τ on the shear band is obtained by equating the macroscopic work rate in the shear band for a single hexagonal cell, $\dot W^P=V_0\tau\dot\gamma$, to the plastic work rate for the hexagonal cell. First note that the vertical bar 3 shortens plastically, and the yield surface for the bar contains a vertex (with zero plastic moment) when the axial force in the bar equals the yield load. The plastic work rate for the shortening bar is $\left(2/\sqrt{3}\right)\sigma_0 t\left|\dot\ell_3\right|$, and the plastic work rate for the unit cell of a single hexagon (of volume V_0) is

$$\dot W^P=V_0\tau\dot\gamma\;=\left(t^2|\dot\omega_2-\dot\omega_1|+2t\left|\dot\ell_3\right|\right)\sigma_0/\sqrt{3}. \tag{A.16}$$

Now make use of (A.14)-(A.16), and the expression (1.1) to obtain the macroscopic shear strength as

$$\frac{\tau}{\bar\rho\,\sigma_0}\approx\frac{2}{3\sqrt{3}}\cos\omega_0\,(\sin\omega_0-\cos 2\omega_0), \tag{A.17}$$

to leading order.

Appendix B: Response of $\omega_0=20°$ honeycomb in tension

The strongly softening tensile response of the non-cavitating filled honeycomb of inclination $\omega_0=20°$ resembles the compressive response of the non-cavitating filled honeycomb of inclination $\omega_0=40°$, compare Figs. 3(a) and 4(a); both figures relate to the primal periodic unit cell response.

Consequently, inclined shear bands are anticipated in the tensile response of a finite specimen of non-cavitating honeycomb of inclination $\omega_0 = 20°$. This case is reported below.

Finite specimen response

Explicit finite element simulations were performed using a specimen of dimension 12 x 27 unit cells of hexagons, of inclination $\omega_0 = 20°$ and a non-cavitating core; consequently, the rectangular specimen is of size 23ℓ x 72ℓ. Again, a single cell is removed at half height on one side to initiate shear bands. The boundary conditions are as given in section 3.1: the top face is subjected to an upward velocity $\dot{u}^\infty/2$ and the bottom face to a downward velocity $-\dot{u}^\infty/2$. Consequently, the specimen is subjected to a constant extension rate $\dot{u}^\infty$.

Representative solutions for the average tensile traction $\langle\sigma^\infty\rangle$ versus non-dimensional extension $\langle u^\infty/\ell\rangle$ are given in Fig. B1(a) for t/ℓ equal to 0.05 and 0.1. A pronounced load peak is observed, followed by a plateau, similar to that observed for the finite specimen of inclination $\omega_0 = 40°$ and non-cavitating core in compression. The evolution of shear bands is shown in Fig. B1(b). The snap-back instability of the specimen is associated with the initiation of a primary shear band at an orientation of $\beta = 55°$ from the imperfection on the left-hand side of the specimen. Thereafter, band broadening of the primary shear band occurs by the formation of additional shear bands of orientation $\beta = 55°$ at the top and bottom faces of the primary shear band. Propagation of the primary shear band across the specimen and band broadening both occur at the same value of macroscopic tensile stress.

Infinite band calculation

Periodic unit cell calculations are performed for the collapse response of an infinite shear band inclined at $\beta = 55°$; the shear band comprises the non-cavitating filled honeycomb of inclination $\omega_0 = 20°$. This calculation closely resembles that reported in section 3.3 for the response of a honeycomb of inclination $\omega_0 = 40°$ in a shear band inclined at $\beta = 40°$. The boundary conditions are as described in section 3.3, but the shear strain rate $\dot{\gamma}$ is now taken to be negative such that the unit cell experiences an extension in the global X_2direction, as indicated in the insert in Fig. B1(c).

Representative results for the shear traction τ versus shear strain γ are shown in Fig. B1(c). The peak shear stress is $\tau_Y = 0.14\bar{\rho}\sigma_0$. Bifurcation into a strongly softening bending mode occurs immediately after the peak load. At a value of shear strain $\gamma \approx 0.25$, the load rises sharply again. A Maxwell construction gives $\sigma_P = 1.0\bar{\rho}^2\sigma_0$ which is only slightly above the observed axial propagation stress for the specimen in Fig. B1(a).

Figure Captions

Figure 1. Geometry and notation. (a) Initial geometry of honeycomb in terms of a Cartesian reference frame, with orthogonal base vectors (e_1, e_2). (b) Deformed configuration. (c) Unit cell used in periodic cell finite element simulations.

Figure 2. (a) Tensile and compressive response of empty periodic unit cell, with inclined bars of inclination $\omega_0 = 20°, 30°$ and $40°$ and t/ℓ=0.05; (b) plastic collapse mechanism in tension and compression by rotation of inextensional hinges; the collapse mode for $\omega_0 = 40°$, t/ℓ=0.05, and, contours of von Mises stress, are shown for (c) tension and (d) compression.

Figure 3. Periodic unit cell in uniaxial tension with an empty core, a core that can cavitate, or a core that cannot cavitate, $t/\ell = 0.05$. (a) Nominal stress versus nominal strain for $\omega_0 = 20°, 30°, 40°$; Deformed configuration are shown for a honeycomb with non-cavitating core for (b) $\omega_0 = 20°$; (c) $\omega_0 = 30°$ and (d) $\omega_0 = 40°$. In each case, the contours are of the von Mises stress.

Figure 4. Periodic unit cell in uniaxial compression, with an empty core, a core that can cavitate, or with a core that cannot cavitate, $t/\ell = 0.05$. (a) Nominal stress versus nominal strain for $\omega_0 = 20°, 30°$ and $40°$; deformed configurations are shown for a honeycomb with a non-cavitating core and (b) $\omega_0 = 20°$; (c) $\omega_0 = 30°$ and (d) $\omega_0 = 40°$.

Figure 5. Compressive collapse mechanisms of a hexagonal honeycomb of initial inclination $\omega_0 = 40°$ for an empty core, cavitating core and a non-cavitating core. The data points refer to finite element simulations for the choice $t/\ell = 0.05$. Contours of ε^{∞} are included in the plot.

Figure 6. Comparison of analytical and finite element predictions of the compressive response of a periodic unit cell of inclination $\omega_0 = 40°$. (a) Cavitating and non-cavitating core for $t/\ell = 0.05$; (b) magnified version of (a) to show early behaviour; (c) non-cavitating core and 3 selected values of t/ℓ; (d) magnified version of (c) to show early behaviour.

Figure 7. Compression of finite specimens with $\omega_0 = 40°$. (a) Geometry of specimens and detail of the defect introduced in all specimens; (b) nominal stress versus nominal strain curve, no cavitation; (c) nominal stress versus nominal strain curves, cavitation allowed, and empty cells. The propagation stress for the no-cavitation specimen is included in (b).

Figure 8. Deformed configurations of finite specimens with $\omega_0 = 40°$ and $t/\ell = 0.1$. (a) Noncavitating core; (b) cavitating core; (c) empty core. Contours in the full specimens represent equivalent plastic strain (von Mises strain) and contours in the close-ups represent normalised von Mises stress, with key as shown.

Figure 9. Maxwell construction of shear band propagation stress. (a) Schematic; (b) geometric construction, the area of I is equal to the area of II; (c) inclined shear band.

Figure 10. (a) Infinite shear band, inclined at $\beta = 40°$ for the $\omega_0 = 40°$ honeycomb and non-cavitating core; (b) deformed state of unit cell; (c) response of unit cell in infinite shear band; (d) magnified portion of unit cell response.

Figure A1. Schematic of the initial collapse mode of non-cavitating honeycomb deforming in a shear band.

Figure B1. Response of filled $\omega_0 = 20°$ honeycomb with non-cavitating core in tension. (a) Finite specimen response for two values of t/ℓ: (b) deformed configuration of the specimen for the choice of $t/\ell = 0.1$; response of unit cell in infinite shear band, inclined at $\beta = 55°$, for two different values of t/ℓ; (d) deformed configurations unit cell in infinite shear band for the choice $t/\ell = 0.05$. Contours in full specimen represent equivalent plastic strain and contours in close-ups and unit cell represent normalised von Mises stress, with key as shown.

Figures

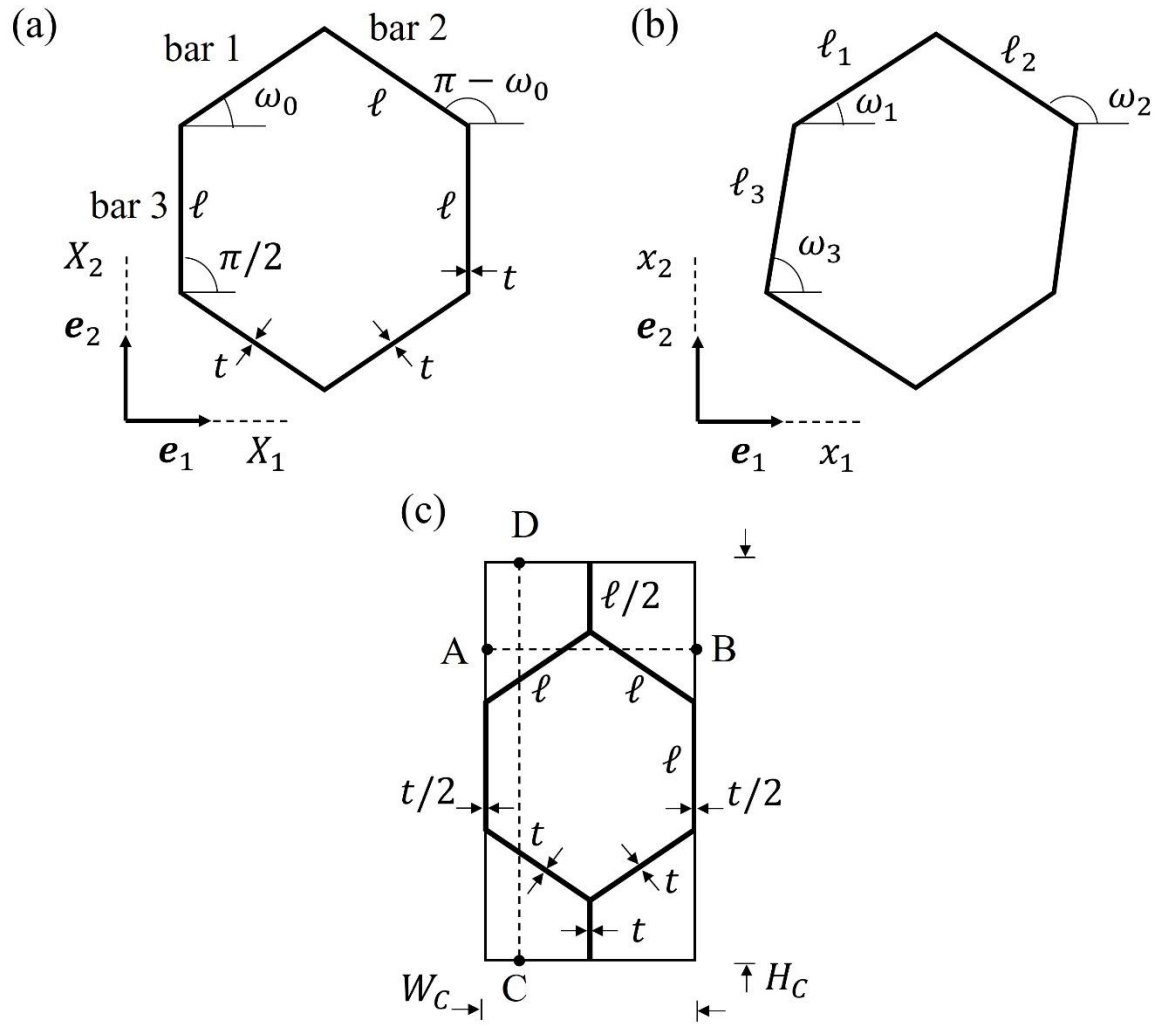

Figure 1. Geometry and notation. (a) Initial geometry of honeycomb in terms of a Cartesian reference frame, with orthogonal base vectors (e_1, e_2). (b) Deformed configuration. (c) Unit cell used in periodic cell finite element simulations.

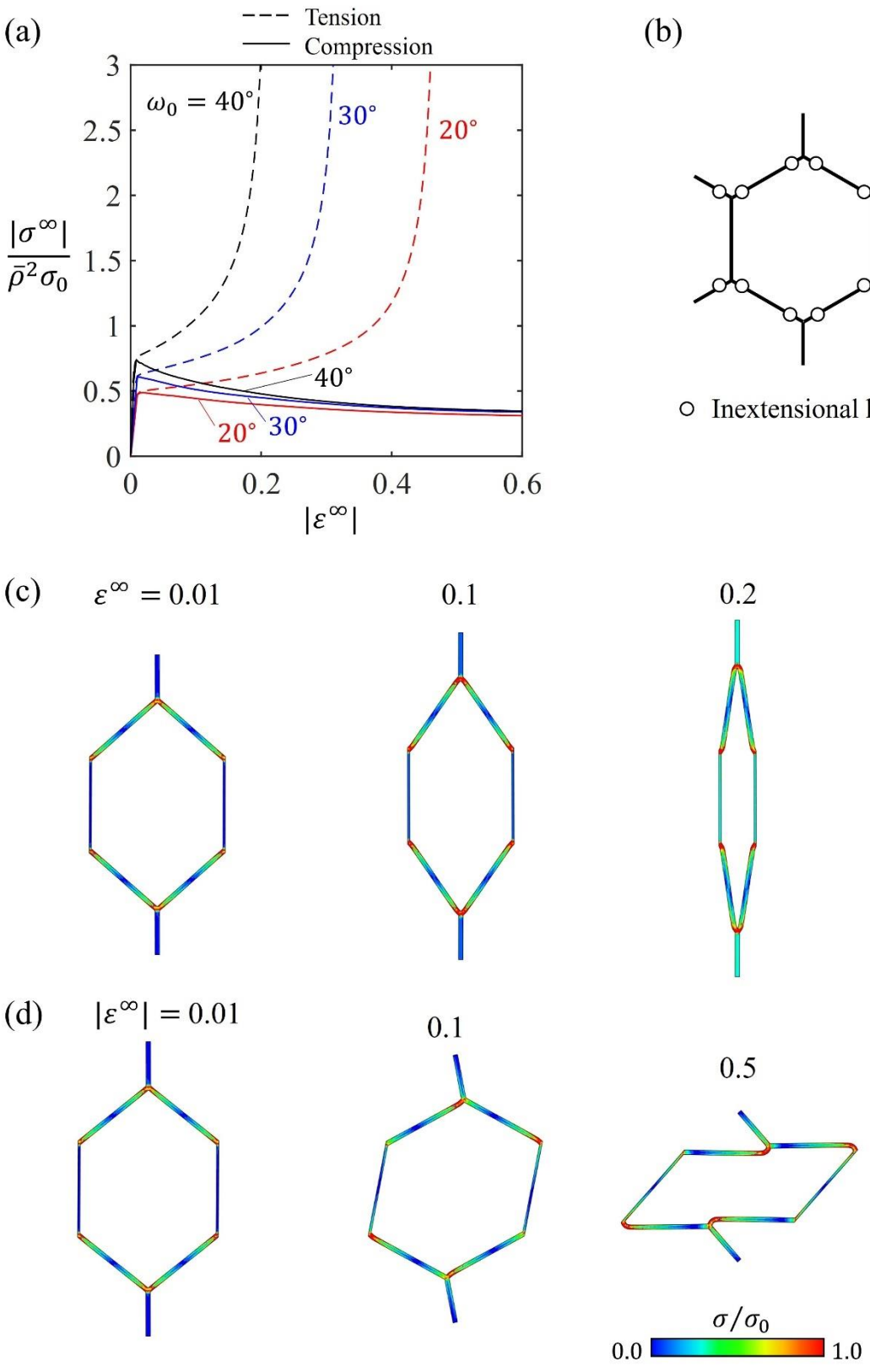

Figure 2. (a) Tensile and compressive response of empty periodic unit cell, with inclined bars of inclination $\omega_0 = 20°, 30°$ and $40°$ and t/ℓ=0.05; (b) plastic collapse mechanism in tension and compression by rotation of inextensional hinges; the collapse mode for $\omega_0 = 40°$, t/ℓ=0.05, and, contours of von Mises stress, are shown for (c) tension and (d) compression.

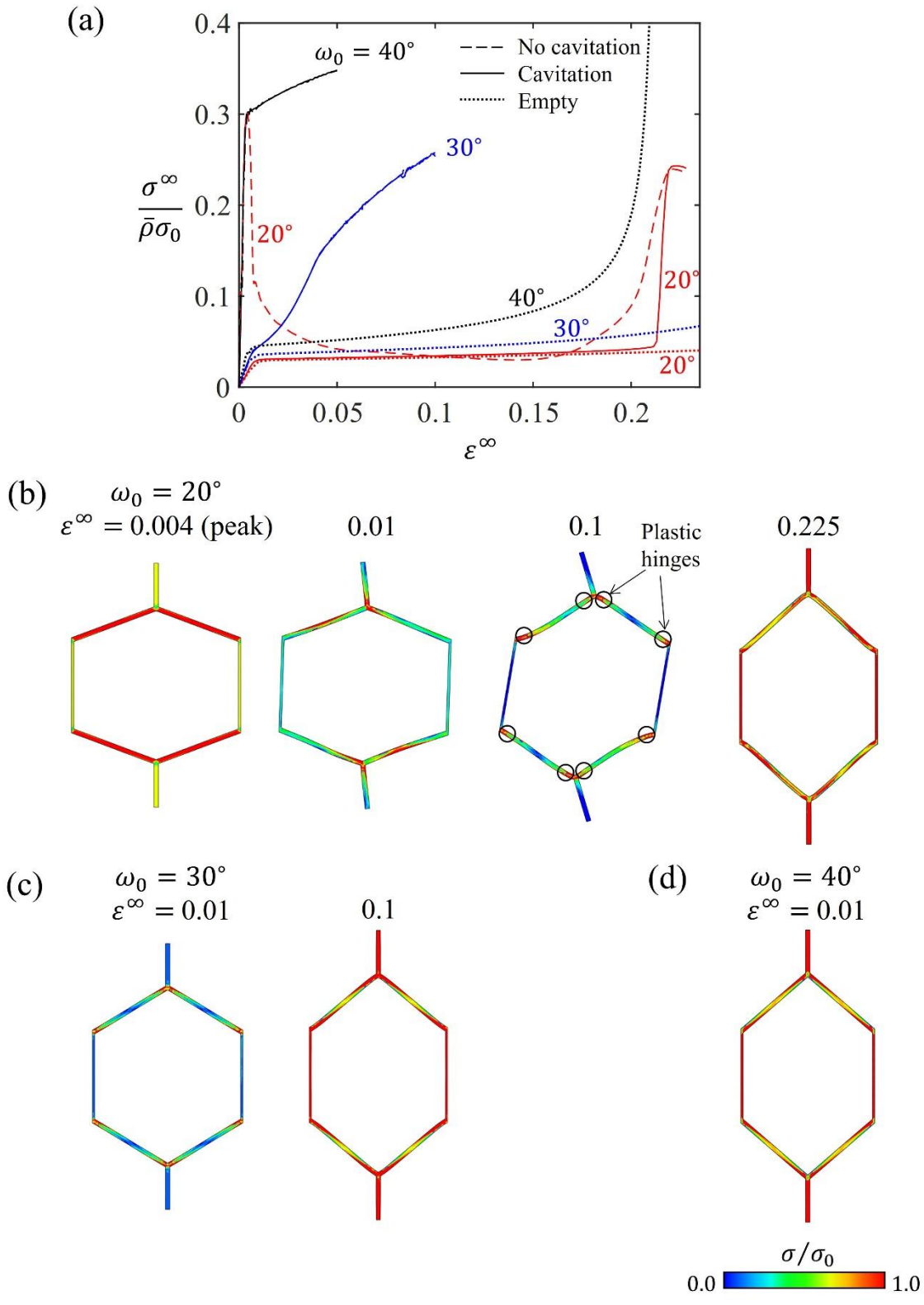

Figure 3. Periodic unit cell in uniaxial tension with an empty core, a core that can cavitate, or a core that cannot cavitate, $t/\ell = 0.05$. (a) Nominal stress versus nominal strain for $\omega_0 = 20°, 30°, 40°$; Deformed configuration are shown for a honeycomb with non-cavitating core for (b) $\omega_0 = 20°$; (c) $\omega_0 = 30°$ and (d) $\omega_0 = 40°$. In each case, the contours are of the von Mises stress.

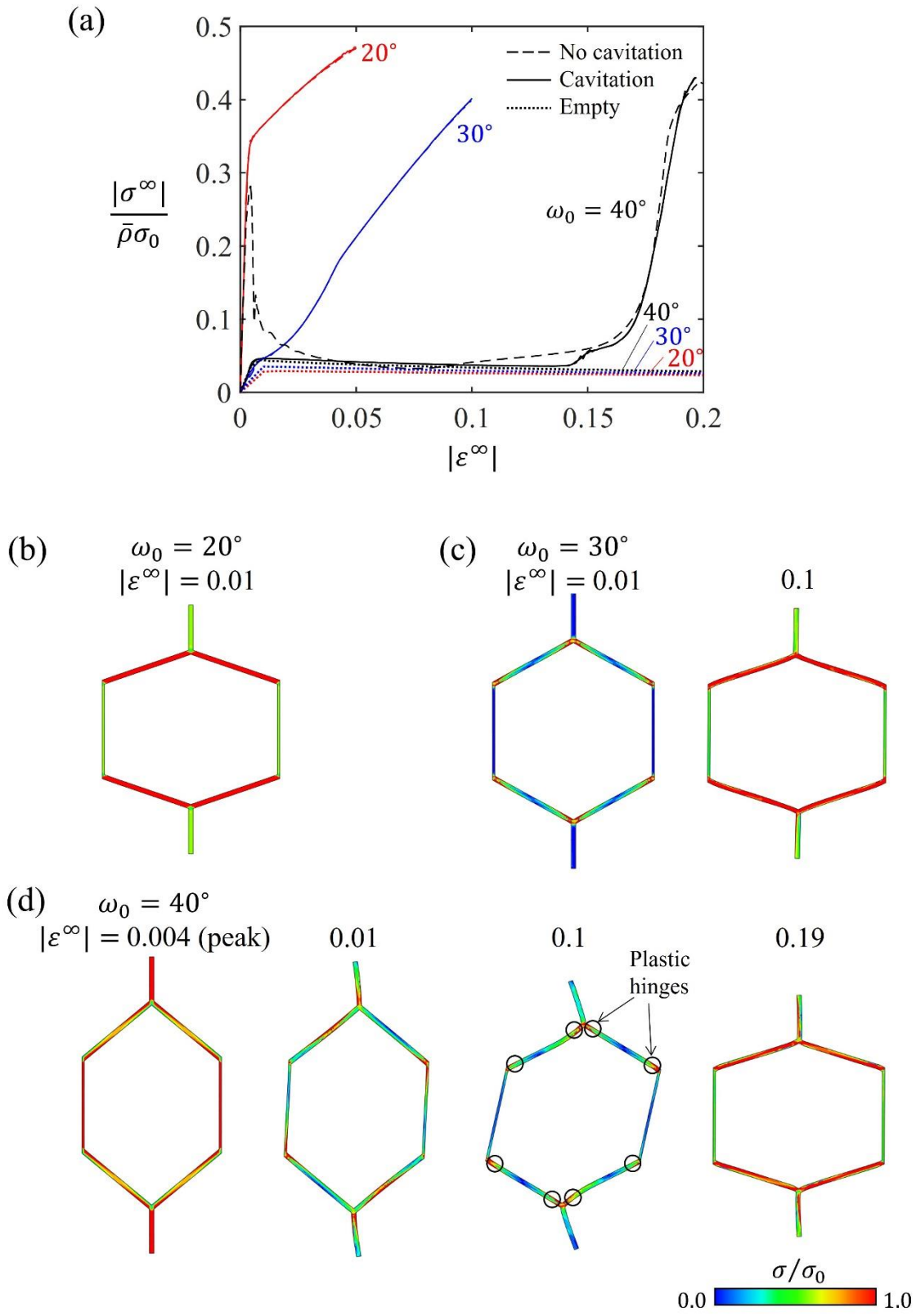

Figure 4. Periodic unit cell in uniaxial compression, with an empty core, a core that can cavitate, or with a core that cannot cavitate, $t/\ell = 0.05$. (a) Nominal stress versus nominal strain for $\omega_0 = 20°, 30°$ and $40°$; deformed configurations are shown for a honeycomb with a non-cavitating core and (b) $\omega_0 = 20°$; (c) $\omega_0 = 30°$ and (d) $\omega_0 = 40°$.

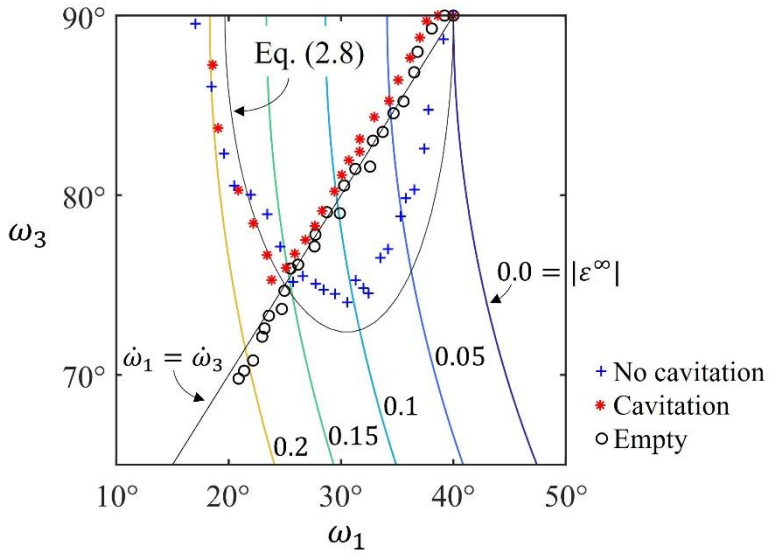

Figure 5. Compressive collapse mechanisms of a hexagonal honeycomb of initial inclination $\omega_0 = 40^\circ$ for an empty core, cavitating core and a non-cavitating core. The data points refer to finite element simulations for the choice $t/\ell = 0.05$. Contours of ε^∞ are included in the plot.

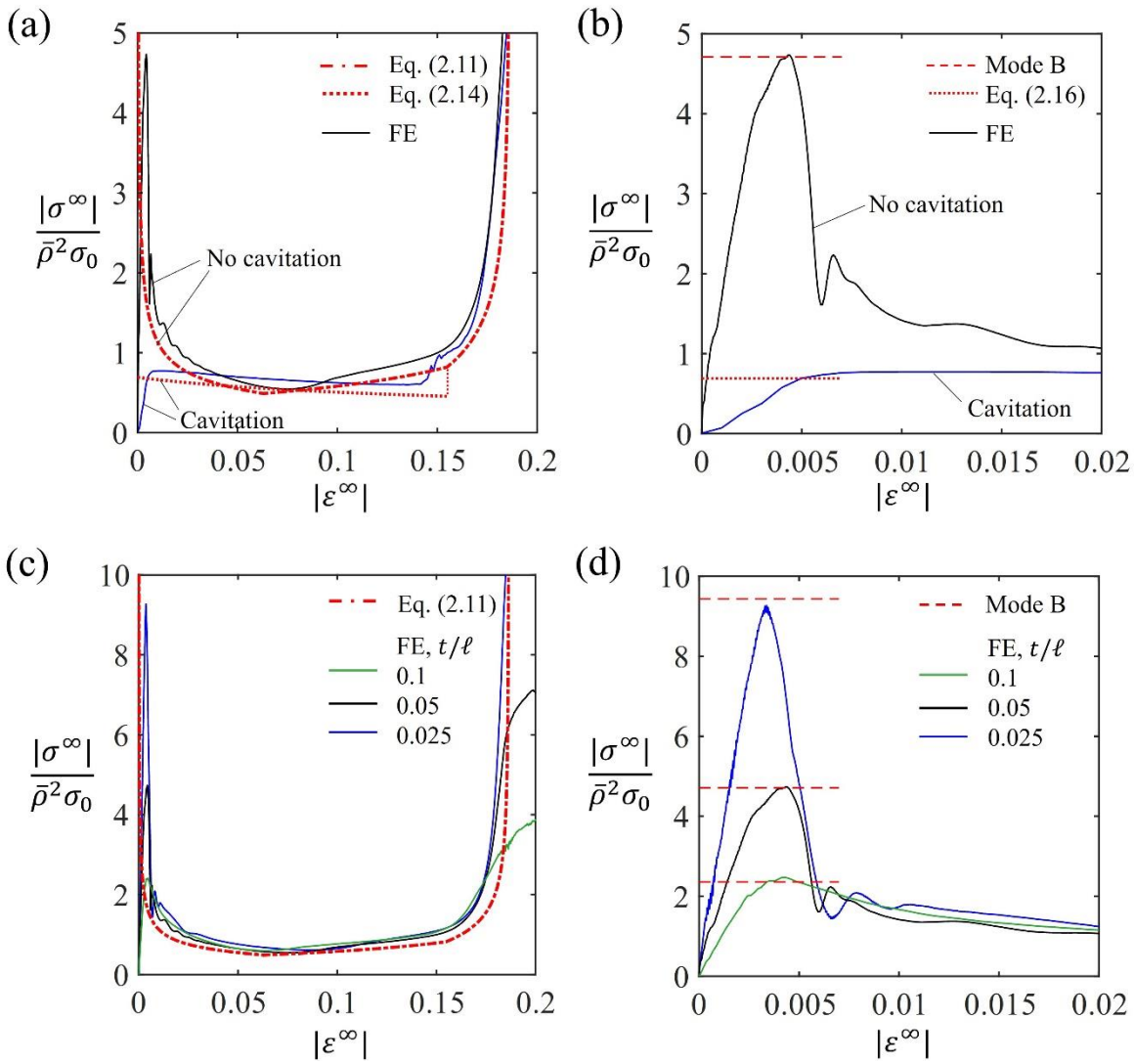

Figure 6. Comparison of analytical and finite element predictions of the compressive response of a periodic unit cell of inclination $\omega_0 = 40°$. (a) Cavitating and non-cavitating core for $t/\ell = 0.05$; (b) magnified version of (a) to show early behaviour; (c) non-cavitating core and 3 selected values of t/ℓ; (d) magnified version of (c) to show early behaviour.

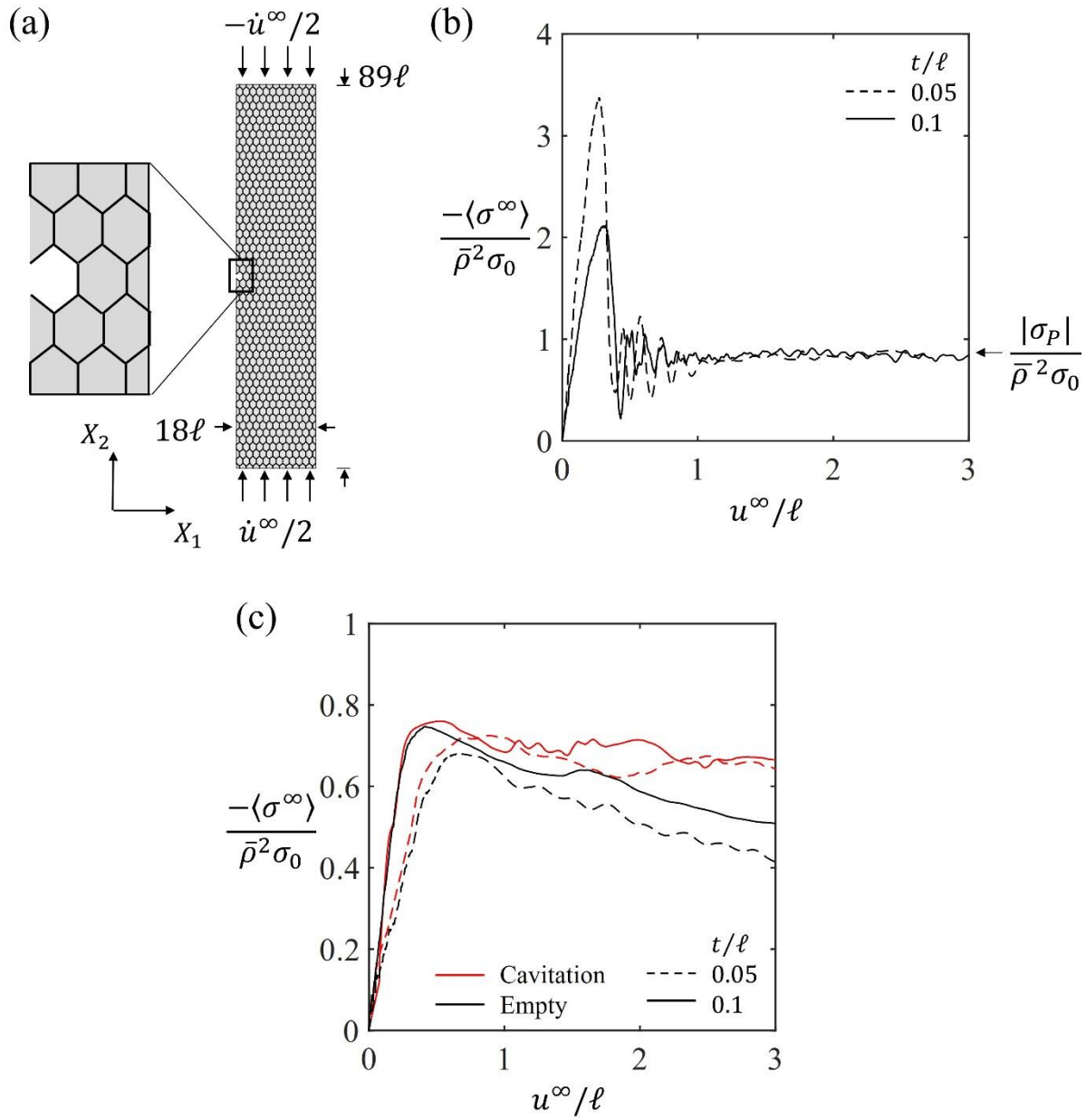

Figure 7. Compression of finite specimens with $\omega_0 = 40°$. (a) Geometry of specimens and detail of the defect introduced in all specimens; (b) nominal stress versus nominal strain curve, no cavitation; (c) nominal stress versus nominal strain curves, cavitation allowed, and empty cells. The propagation stress for the no-cavitation specimen is included in (b).

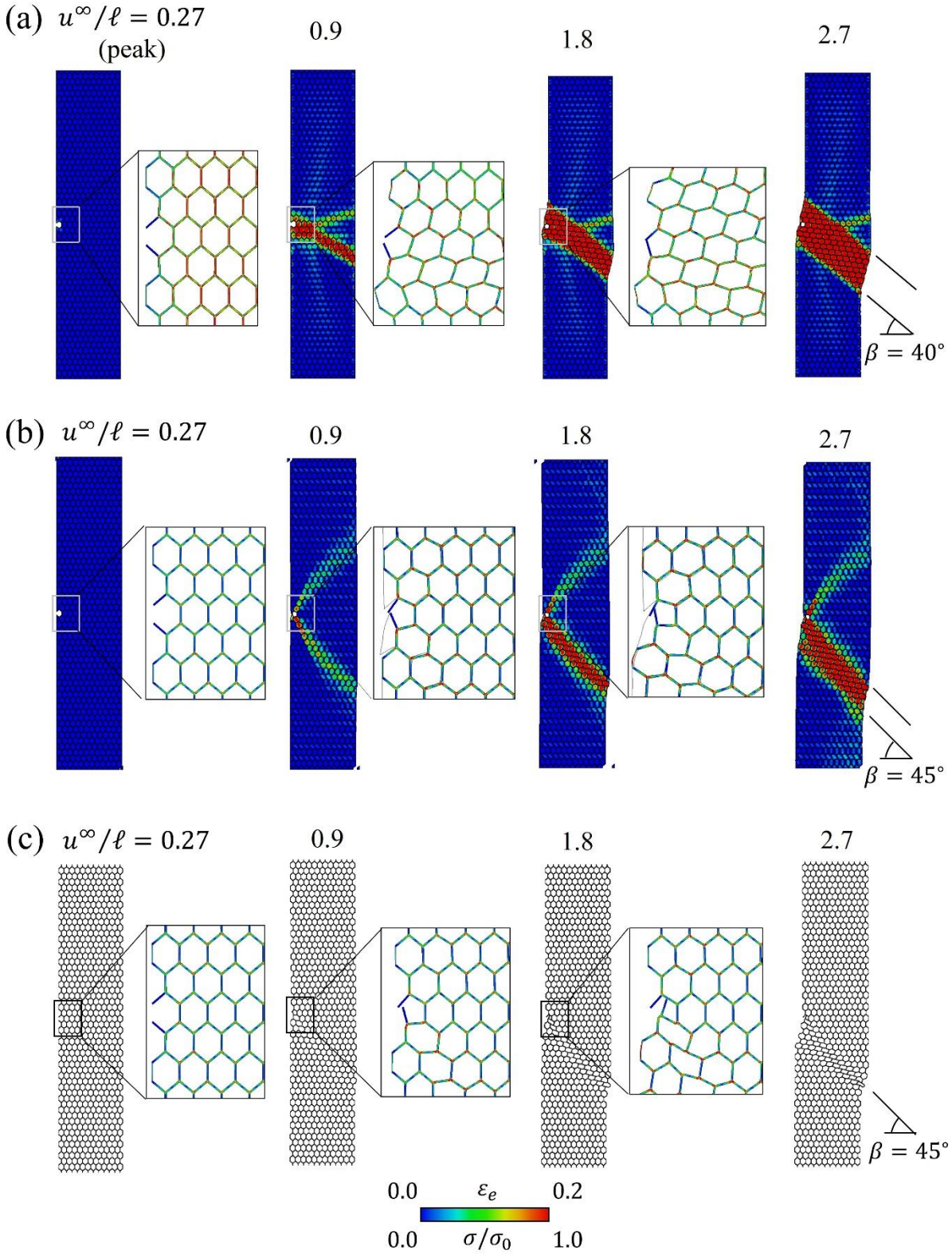

Figure 8. Deformed configurations of finite specimens with $\omega_0 = 40°$ and $t/\ell = 0.1$. (a) Noncavitating core; (b) cavitating core; (c) empty core. Contours in the full specimens represent equivalent plastic strain (von Mises strain) and contours in the close-ups represent normalised von Mises stress, with key as shown.

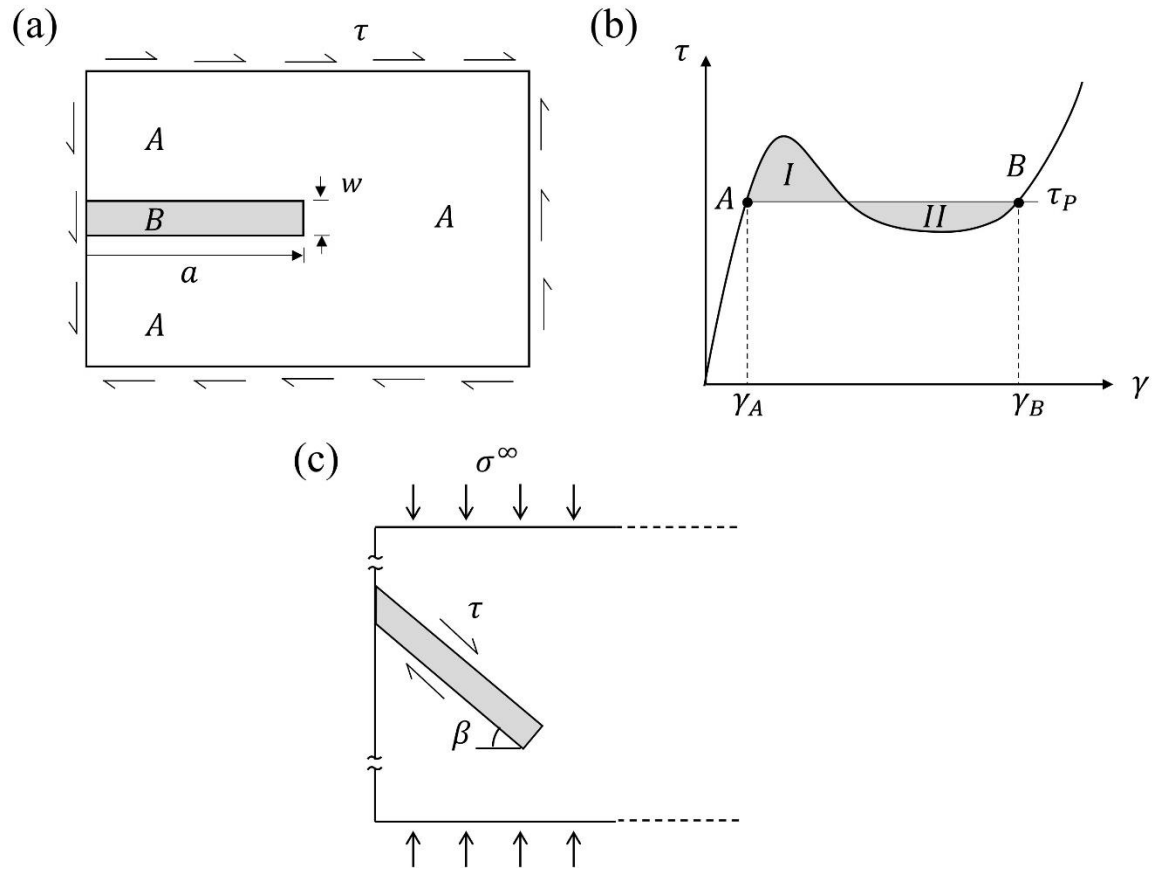

Figure 9. Maxwell construction of shear band propagation stress. (a) Schematic; (b) geometric construction, the area of I is equal to the area of II; (c) inclined shear band.

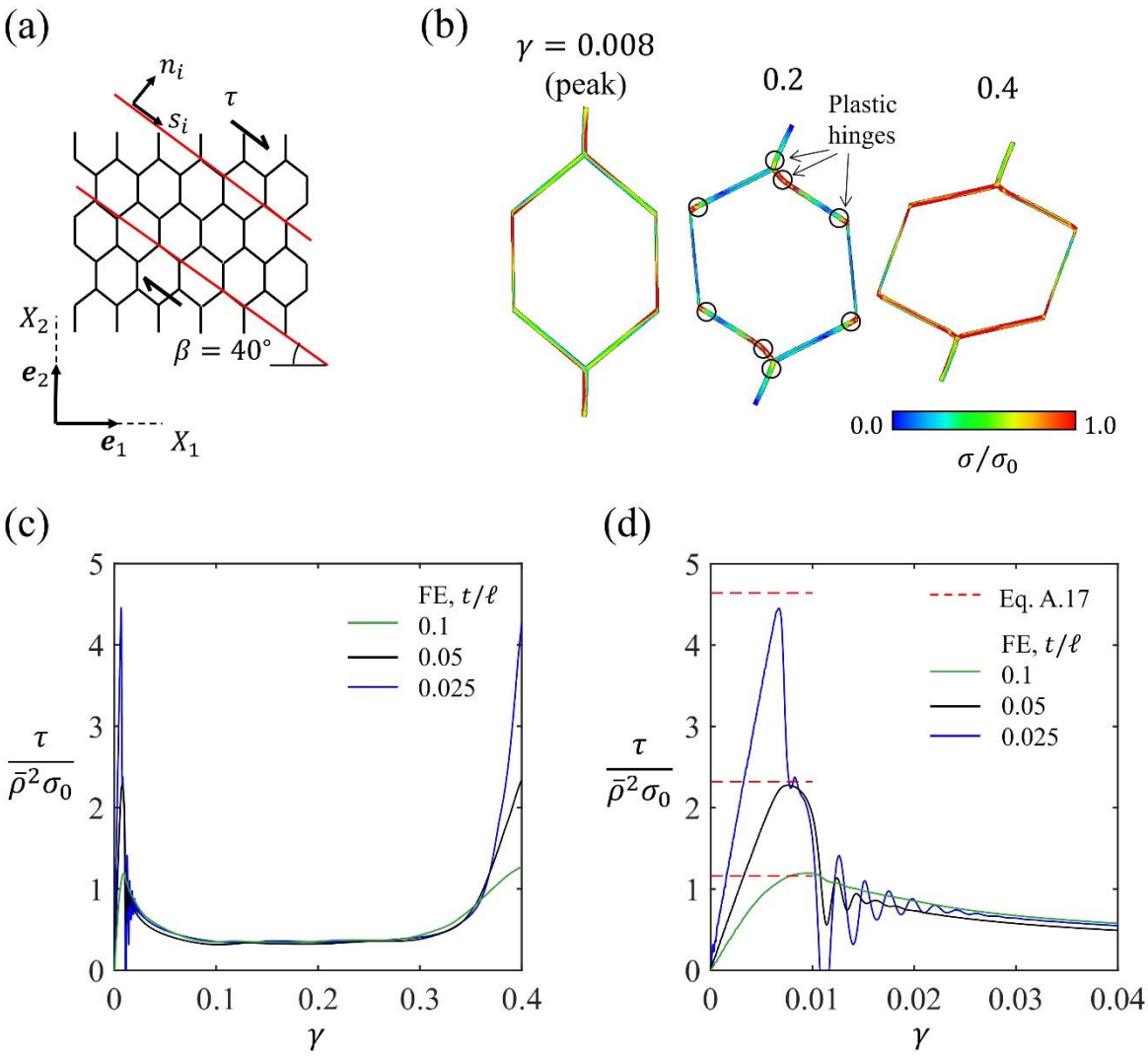

Figure 10. (a) Infinite shear band, inclined at $\beta = 40°$ for the $\omega_0 = 40°$ honeycomb and non-cavitating core; (b) deformed state of unit cell; (c) response of unit cell in infinite shear band; (d) magnified portion of unit cell response.

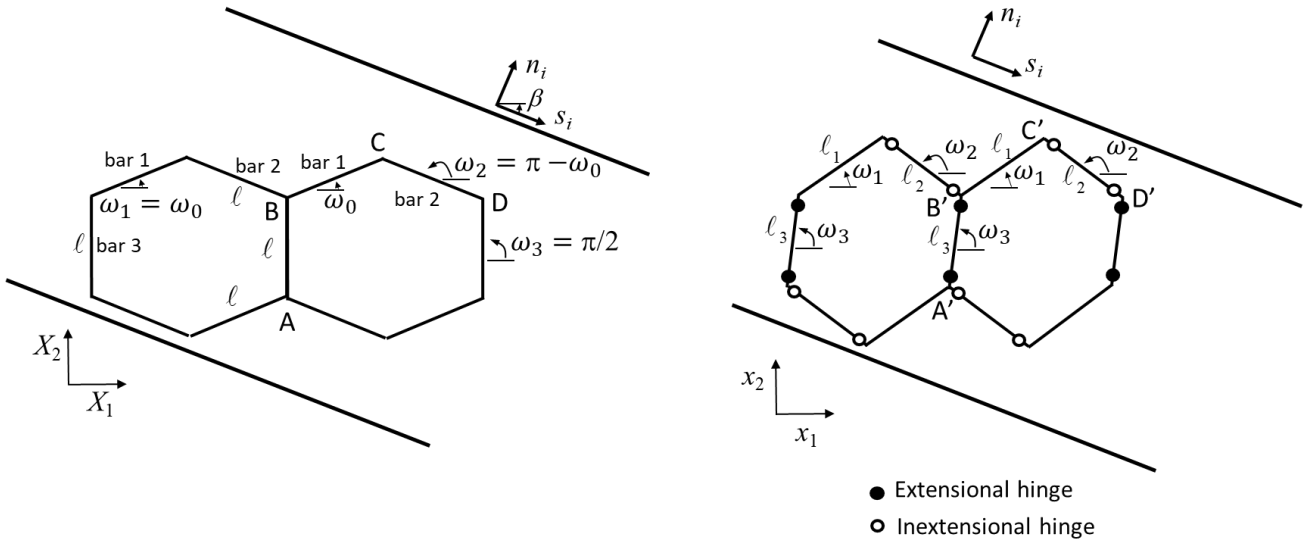

Figure A1. Schematic of the initial collapse mode of non-cavitating honeycomb deforming in a shear band.

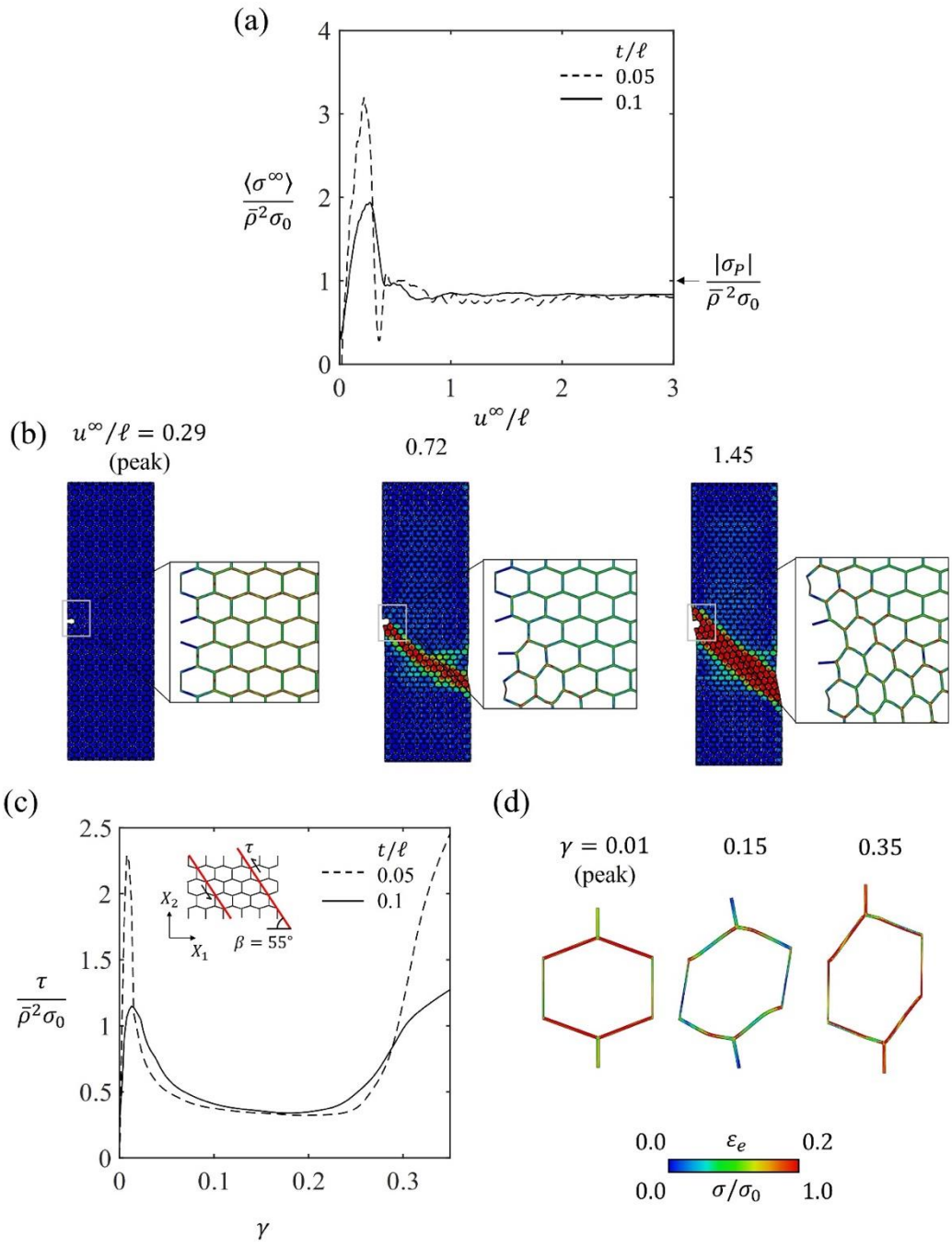

Figure B1. Response of filled $\omega_0 = 20°$ honeycomb with non-cavitating core in tension. (a) Finite specimen response for two values of t/ℓ: (b) deformed configuration of the specimen for the choice of $t/\ell = 0.1$; response of unit cell in infinite shear band, inclined at $\beta = 55°$, for two different values of t/ℓ; (d) deformed configurations unit cell in infinite shear band for the choice $t/\ell = 0.05$. Contours in full specimen represent equivalent plastic strain and contours in close-ups and unit cell represent normalised von Mises stress, with key as shown.